

Article

A Hybrid Model Based on A Modified Optimization Algorithm and An Artificial Intelligence Algorithm for Short-Term Wind Speed Multi-Step Ahead Forecasting

Zonggui Yao ¹ and Chen Wang ^{2,*} 

¹ School of Computer Science and Technology, Hangzhou Dianzi University, Hangzhou 310018, China; yaozonggui_00@hdu.edu.cn

² School of Information Science & Engineering, Lanzhou University, Lanzhou 730000, China

* Correspondence: chenwang15@lzu.edu.cn; Tel.: +86-0571-86919093

Received: 22 March 2018; Accepted: 26 April 2018; Published: 5 May 2018



Abstract: In the last few years, researchers have paid increasing attention to improving the accuracy of wind speed forecasting because of its vital impact on power dispatching and grid security. However, it is difficult to achieve a good forecasting performance due to the randomness and intermittency characteristics of wind speed time series. Current forecasting models based on neural network theory could adapt to various types of time series data; however, these models ignore the importance of data pre-processing and model parameter optimization, which leads to poor forecasting accuracy. In this paper, a new hybrid model is developed for short-term multi-step wind speed forecasting, which includes four modules: (1) the data pre-processing module; (2) the optimization module; (3) the hybrid nonlinear forecasting module and (4) the evaluation module. In order to estimate the forecasting ability of the proposed hybrid model, 10 min wind speed data were applied in this paper as a case study. The experimental results in six real forecasting cases indicate that the proposed hybrid model can provide not only accurate but also stable performance in terms of multi-step wind speed forecasting can be considered an effective tool in planning and dispatching for smart grids.

Keywords: wind speed multi-step forecasting; data pre-processing; modified optimization algorithm; neural networks

1. Introduction

Wind energy, as one of the most promising renewable energy resources (RESs), has gradually become a remarkable alternative resource to fossil energy due to being non-polluting, environmentally friendly cost effective [1]. In the past few decades, as a result of policy-driven environmental and energy security concerns, it has become the fastest-growing RES for power generation and has attracted more and more attention worldwide [2]. In late 2016, the Global Wind Energy Council (GWEC) reported that more than 54.6 GW of global wind power capacity was added in 2016, which represents a growth rate of 11.8% and means that the global installed capacity of wind turbines can generate approximately 5% of electricity demand worldwide [3]. However, due to the intermittency and uncertainty inherent to wind sources, the wholesale integration of wind power into the traditional grid system presents a significant challenge in terms of reducing cost and improving reliability in power system operation [4]. Therefore, with the goal of moderating the negative impacts and increasing the utilization efficiency of wind power conversion, it is necessary to increase the accuracy of wind speed forecasting [5].

During recent years a number of technologies have been proposed in the literature for increasing the accuracy of wind speed forecasting, which can be classified into four categories: physical models, statistical models, spatial correlation models, artificial intelligence models [6]. The physical forecasting models are generally based on terrain features, atmospheric pressure, ambient temperature, other meteorological information to obtain an evaluation of the considered site's wind speed forecasting. These models are very effective for medium-term and long-term wind speed forecasting because of the many relevant variables they include [7]. However, these physical-based approaches require considerable observed data with a limited simulation scale always have a higher cost [8]. In contrast, statistical forecasting models, which include the Auto Regressive Moving Average (ARMA) [9], Auto Regressive Integrated Moving Average (ARIMA) [10], Generalized Autoregressive Conditional (GARCH) [11], are more suitable for handling time series forecasting are simple to implement by utilizing a set of historical data. This makes these techniques time saving in building models. However, statistical models cannot deal with the non-linearity that exists in wind speed time series because of their linear correlation structure [12]. Typically, spatial correlation models primarily utilize the spatial relationships between wind speeds at different sites. In some cases, they can achieve satisfactory prediction accuracy [13]. However, their information requirements, including wind speed and delay times, add complexity and cost to their implementation [6]. With the rapid development of soft-computing techniques, some artificial intelligence approaches are widely used for wind speed forecasting in various fields [14,15], such as artificial neural networks (ANNs), support vector machines (SVMs), fuzzy logical based models [6]. Among these approaches, the most prevalent intelligent wind speed forecasting models are based on ANNs, which including the back propagation (BP) neural network [16], general regression neural network (GRNN) [17], radial basis function neural network (RBFNN) [18] and deep belief network (DBN) [19], among others. These models possess the ability to structure the relationship between input data and output data with higher data error tolerance perform well in non-linear time series forecasting [16]. Nevertheless, the main drawbacks of individual artificial intelligence models are that they may easily get into local optimum and exhibit a relatively low convergence rate due to the random network initial weights and thresholds [19]. From the above discussion, it can be seen that each model has its own specific benefits and drawbacks we summarize the merits and demerits of the four types of wind speed models in Table 1.

Table 1. Theoretical comparison of the strengths and disadvantages exist in present individual wind speed forecasting models.

| The Type of the Model | Main Methods | The Features and Strengths of Each Model | The Disadvantages of Each Model |
|---------------------------------------|--|--|--|
| <i>Physical models</i> | Mesoscale numerical model; Computational fluid dynamics method [7] | Obtaining good performance in the long-term forecasting; Having a high parallel efficiency [7]. | Requiring considerable observed data with limited simulation scale; Having higher cost [8]. |
| <i>Statistical models</i> | Time series approach [9–11] | A wide application and cost less time to build models [12]. | Obtaining poor performance in dealing with non-linear time series forecasting [12]. |
| <i>Spatial correlation models</i> | Spatial correlation models [13] | Obtaining a satisfactory wind speed forecasting by vast quantities of information that need be considered and collected [13]. | Requiring wind speed measurements from multiple spatial correlated sites so that the implementation has difficulty due to the measurements and their time delays [6]. |
| <i>Artificial intelligence models</i> | Neural network approach; Support vector machine; Fuzzy and clustering approach [6,15–19] | Having a high ability of fault tolerance do not require accurate mathematical models with each man-machine interaction; Obtaining a satisfactory performance in non-linear time series forecasting [18] | Easily getting into local optimum, over-fitting and exhibiting the relatively low convergence rate; Having a relatively low accuracy and lack for systematization [19]. |

Due to the inherent weaknesses of each model, as well as the intermittency and complex fluctuations of wind speed, individual forecasting models cannot always capture the characteristics of a time series, especially when it comes to the non-linear traits of wind speed. Thus, in order to obtain more accurate wind speed forecasting, as well as overcome the shortcomings in the individual models, some hybrid models which incorporate the individually superior features of various algorithms have been developed. In recent years, with the aim of obtaining promising forecasting results, many hybrid models for wind speed forecasting have been successfully developed and have improved the accuracy of forecasting to some degree. For instance, Cadenas et al. [20] proposed a hybrid model, which consists of ARIMA models and ANN models for wind speed forecasting. The results showed that the forecasting achieved with this hybrid outperformed the individual ARIMA and ANN models in three experimental sites in Mexico. Liu et al. [21] developed a hybrid model for wind speed forecasting based on the theories of wavelet, wavelet packet, time series analysis artificial neural networks. The results of three simulation cases indicated that the proposed hybrid model achieved a satisfactory performance in wind speed forecasting. Du et al. [22] developed a wind speed forecasting model based on certain confidence and fluctuation characteristics for 10 min wind speed forecasting at three wind farms in Penglai Shandong Province, eastern China. The experiments indicated that the developed hybrid model can obtain more accurate forecasting results compared with other alternative models. Ma et al. [23] proposed a model based on a de-noising approach with a dynamic fuzzy neural network to improve the accuracy of wind speed forecasting. Three experimental results demonstrated that the model satisfactorily approximated the observed wind speed value. Wang et al. [24] developed an ensemble empirical mode decomposition (EEMD), genetic algorithm (GA), BP neural network for wind speed forecasting. In this proposed hybrid model, the EEMD is employed to analyze and de-noise the nonlinear stochastic signals the BP neural network, optimized by GA (GA-BP), is developed for dealing with each of the decomposed sub-series. The experimental results from a wind farm in Inner Mongolia, China, indicated that the proposed hybrid model can provide more accurate wind speed forecasting than a traditional wavelet neural network, including both the GA-BP and GA-BP with EMD (EMD-GA-BP) models. Ren et al. [25] developed hybrid wind speed forecasting by integrating EMD and a support vector machine (SVR). Several intrinsic mode functions (IMFs) and a residue handled by EMD were separately generated to train the SVR. The case studies showed that the proposed EMD-SVR model outperformed other alternative models involved in their research with respect to computational complexity and accuracy. Zhang et al. [26] presented a hybrid model based on EMD, feature selection with ANN and SVM yield for short-term wind speed forecasting. The results of their study demonstrated that the proposed hybrid approach achieved a satisfactory performance in dealing with wind speed forecasting using three real datasets in China. Zhang et al. [27] developed a hybrid model which combined an extreme learning machine (ELM), based on feature selection parameters optimized by using a hybrid backtracking search algorithm (HBSA). The developed hybrid model was applied to data from two wind farms in Inner Mongolia, China, Sotavento Galicia, respectively. The experimental results indicated that the hybrid model was able to capture the non-linear features of a wind speed series and thus achieve a more promising forecasting performance.

The previous research indicates that there is still no one approach that can provide an elegant solution to wind speed forecasting. Model performance under specific circumstances should be analyzed and understood then incremental improvements should be made based upon the knowledge that is gained [28]. Thus, obtaining a satisfactory wind speed forecasting performance is still a difficult and challenging task it is necessary to further exploit more efficient and accurate models in the field of wind speed forecasting. Due to these factors, a novel wind speed forecasting model which combines wavelet de-noising (WD), a modified ant colony optimization algorithm, BP neural networks (WD-APSOACO-BP) is developed in this paper. The developed hybrid model consists of four modules: a data pre-processing module, an optimization module, a forecasting module, a comprehensive evaluation module. In the data pre-processing module, the WD technique is employed to extract the basic characteristics from the non-stationary wind speed time series fractal extrapolation is used to

handle the missing data. The optimization module includes use of a modified adaptive particle swarm optimization algorithm-based ant colony optimization algorithm (APSOACO), which is adopted to optimize the weights and thresholds of individual BP neural networks and overcome the drawbacks of the BP algorithm in terms of converging on a local optimum when the training surface has a multimodal distribution. In this way, we aimed to further improve the forecasting accuracy. In the forecasting module, the hybrid forecasting APSOACO-BP model is established as a forecasting engine for wind speed forecasting. After completing the steps above, the evaluation module is adopted to synthetically assess the developed hybrid wind speed forecasting system. This module consists of the evaluation criteria, forecasting validity, a population stability index four experiments designed in six wind speed sites using time series from the Shandong province of China as well as a comprehensive analysis of these experiments. The significant contributions of this study are summarized as follows:

- (1) Given that the wind speed exhibits uncertainty and randomness, a valid mathematical data preprocessing module, which was derived from the theory of signal time-frequency localization, is adopted to decompose the original wind speed time series into a number of sub-series. This module can effectively de-noise and fully extract the main features of a wind speed time series thus improves the forecasting accuracy.
- (2) A novel modified optimization algorithm, the APSOACO, is proposed to optimize the initial weights and thresholds of the BP neural network, due to its better convergence performance and lower number of required iterations compared with individual traditional optimization algorithms. This module not only provides a new option for solving problems such as computational complexity and easy trapping into a local optimal solution that traditional forecasting engines may encounter also makes a contribution to improving the accuracy of wind speed forecasting.
- (3) In order to estimate the overall performance of the developed hybrid model, a more scientific and comprehensive evaluation module is developed in this paper. This module not only sufficiently analyzes both the accuracy and stability of forecasting results also discusses the effectiveness of the proposed model in terms of the performance of the employed optimization algorithm and wavelet function.
- (4) With the aim of improving the quality of wind speed data and further enhancing the forecasting accuracy, an effective data interpolation technique and a rolling mechanism were also adopted in this paper. These techniques possess the capacity to enrich and improve the information of wind speed observations, which can in turn provide more accurate and stable wind speed forecasting.

The rest of this paper is organized as follows: Section 2 presents a brief description of related methodology. Section 3 describes the back propagation neural network optimized by different heuristic algorithms and describes the structure of the proposed integrated forecasting framework. Six real experiments and their corresponding results are presented in Section 4. The forecasting validity of the proposed hybrid model is discussed in Section 5. Finally, the conclusion of this research is given in Section 6.

2. Methodology

Before utilizing the proposed hybrid model for wind speed forecasting, it is necessary to introduce some of the significant components. Therefore, some operating theories—including the wavelet de-noise algorithm, the fractal interpolation the single nonlinear neural network—are concisely introduced in this section.

2.1. The Wavelet De-Noise Technique

The wavelet transform is a time-frequency representation of a signal. It can be used for noise reduction, feature extraction, or signal compression, for example [29]. It is an essential tool for data pre-processing and has been widely utilized in de-noising and for extracting the basic characteristics

from a non-stationary time series. This type of algorithm can be divided into two categories: continuous wavelet transforms (CWTs) and discrete wavelet transforms (DWTs).

In continuous wavelet transforms, a given signal of finite energy is projected onto a continuous family of frequency bands (or similar subspaces of the L^p function space $L^2(\mathbf{R})$). For instance, the signal may be represented on every frequency band of the form $[f, 2f]$ for all positive frequencies $f > 0$. Then, the original signal can be reconstructed by a suitable integration of all the resulting frequency components.

The frequency bands or subspaces (sub-bands) are scaled versions of a subspace at scale 1. This subspace is in most situations generated by the shifts of one generating function ψ in $L^2(\mathbf{R})$, the mother wavelet. For the example of the scale 1 frequency band $[1,2]$ this function is:

$$\psi(t) = 2 \sin c(2t) - \sin c(t) = \frac{\sin(2\pi t) - \sin(\pi t)}{\pi t}$$

In discrete wavelet transforms it is computationally impossible to analyze a signal using all the wavelet coefficients, so one may wonder if it is sufficient to pick a discrete subset of the upper halfplane to be able to reconstruct a signal from the corresponding wavelet coefficients. One such system is the affine system for some real parameters $a > 1, b > 0$. The corresponding discrete subset of the halfplane consists of all the points $(a^m, na^m b)$ with m, n in \mathbf{Z} . The corresponding child wavelets are now given as:

$$\psi_{m,n}(t) = \frac{1}{\sqrt{a^m}} \psi\left(\frac{t - nb}{a^m}\right)$$

A sufficient condition for the reconstruction of any signal x of finite energy is given by the formula:

$$x(t) = \sum_{m \in \mathbf{Z}} \sum_{n \in \mathbf{Z}} \langle x, \psi_{m,n} \rangle$$

in which the functions $\{\psi_{m,n}: m, n \in \mathbf{Z}\}$ form an orthonormal basis of $L^2(\mathbf{R})$.

This separates the signal into components at various scales corresponding to successive frequencies. It can be noted that the DWT corresponds to the multi-resolution approximation expressions, which can analyze a signal in a number of frequency bands (or at a number of scales) [30,31].

2.2. The Artificial Neural Network Model and Fractal Representation

Backpropagation is a method used in artificial neural networks to calculate a gradient that is needed in the calculation of the weights to be used in the network, which is a powerful algorithm for apportioning error responsibility through a multi-layer network was formulated in the form of the backpropagation algorithm. The backpropagation algorithm employs the Delta Rule, calculating error at output units in a manner to that used in structure of neural network, while error at neurons in the layer directly preceding the output layer is a function of the errors on all units that use its output. The effects of error in the output node(s) are propagated backward through the network after each training case. The essential idea of backpropagation is to combine a non-linear multi-layer perceptron-like system capable of making decisions with the objective error function of the Delta Rule [32]. As a result, BP neural network is selected as a forecaster to integrate the hybrid model in this study. It is based on a gradient descent method that minimizes the sum of the squared errors between the actual and desired output values. The transfer function is of the neuron type (commonly referred to as the activation function [33]). The output function is between 0 and 1 and can transform input to output for continuous nonlinear mapping.

Definition 1. *Neural network models in artificial intelligence are usually referred to as artificial neural networks (ANNs). These are essentially simple mathematical models defining a function $f: XY$ or a distribution over*

X or both X and Y sometimes models are also intimately associated with a particular learning algorithm or learning rule.

In order to eliminate the difference of each variable, the input and output data of the neural network should be normalized the normalization formula is as follows:

$$X' = 2 \times \frac{X_i - X_{i,\min}}{X_{i,\max} - X_{i,\min}} - 1, \quad (i = 1, 2, \dots, n) \quad X' \in [-1, 1]$$

where X' is the normalized data. $X_{i,\min}$ and $X_{i,\max}$ are the minimum and maximum value of actual data vectors and X_i denotes the actual data.

Step 1. Calculate outputs of all hidden layer nodes.

$$y_j = f\left(\sum_i \omega_{ji}x_i + b_j\right) = f(\text{net}_j) \quad (i = 1, \dots, n; j = 1, \dots, 2n)$$

$$\text{net}_j = \sum_i \omega_{ji}x_i + b_j \quad (j = 1, \dots, 2n)$$

where the activation value of node j is net_j , ω_{ji} represents the connection weight from input node i to hidden node j , b_j represents the threshold of neuron j , y_j represents the output of hidden layer node j . f is the activation function of a node, which is usually a sigmoid function.

$$f(x) = \frac{1}{1 + e^{-x}}$$

Step 2. Calculate the output data of the neural network.

$$O_1 = f\left(\sum_i \omega_{oj}y_i + b_o\right) \quad (i = 1, \dots, n; j = 1, \dots, 2n)$$

where ω_{oj} represents the connection weight from hidden node j to the output node, b_o represents the threshold of the neuron, O_1 represents the output data of the network. f_o is the activation function of the output layer node.

Step 3. Minimize the global error via the training algorithm.

$$\text{Mean square error} = \frac{1}{t} \sum (O_1 - R_t)^2$$

where R_t is the real output of the training data in Equation.

2.3. Fractal Interpolation

The fractal interpolation technique was developed by Barnsley and Harrington and provides benign deterministic representation for complicated phenomena [34]. The fractal interpolation function is defined as fixed points of the map between function spaces using iterated function systems (IFSs). The details of the fractal interpolation is as follows:

Theorem 1. Let $[x_0, x_N] \subset \mathbb{R}$ be an interval and $x_0 < x_1 < \dots < x_{i-1} < x_i < \dots < x_N$ be a subdivision of this interval ($N \geq 2$). Let $F_i \in \mathbb{R}$ ($i = 0, 1, \dots, N$) be some arbitrary value attached to the point x_i which is to be interpolated over the interval $[x_0, x_N]$ by a continuous function $f: [x_0, x_N] \rightarrow \mathbb{R}$ with $f(x_i) = F_i$ ($i = 0, 1, \dots, N$).

Let $u_i: [x_0, x_N] \rightarrow [x_{i-1}, x_i]$ be the invertible maps:

$$u_i(x) = \frac{x_i - x_{i-1}}{x_N - x_0}x + \frac{x_N x_{i-1} - x_0 x_i}{x_N - x_0} \quad (i = 0, 1, \dots, N)$$

Let $\alpha_i \in \mathbb{R}$ ($i = 0, 1, \dots, N$) be any given number (called the vertical scaling factors) with $0 < |\alpha_i| < 1$ and $h_i: [x_0, x_N] \rightarrow \mathbb{R}$ be the linear functions.

$$h_i(x) = \left(\frac{F_i - F_{i-1}}{x_N - x_0} - \alpha_i \frac{F_N - F_0}{x_N - x_0} \right) x + \frac{x_N F_{i-1} - x_N F_i}{x_N - x_0} - \alpha_i \frac{x_N F_0 - F_N}{x_N - x_0} \quad (i = 0, 1, \dots, N)$$

For $i = 0, 1, \dots, N$.

Then there exists a unique continuous function $f: [x_0, x_N] \rightarrow \mathbb{R}$ with $f(x_i) = F_i$ ($i = 0, 1, \dots, N$) such that the following condition holds true:

$$f(u_i(x)) = \alpha_i f(x) + h_i(x) \text{ for } x \in [x_0, x_N] \text{ and } i = 0, 1, \dots, N$$

Proof. Let $\mathcal{F} = \{g: [x_0, x_N] \rightarrow \mathbb{R} \text{ be continuous with } g(x_0) = F_0, g(x_N) = F_N\}$. \mathcal{F} is a complete metric space with the maximum metric. Define the operator $T: \mathcal{F} \rightarrow \mathcal{F}$ piecewise by:

$$T(g)(y) = \alpha_i g(u_i^{-1}(y)) + h_i(u_i^{-1}(y)) \text{ for } x \in [x_0, x_N] \text{ and } i = 0, 1, \dots, N$$

Then, $T(g)$ is well defined and $T(g)(x_i) = F_i$ $i = 0, 1, \dots, N$. This operator is a contraction and its unique fixed point is the function f . \square

2.4. Rolling Mechanism Based Multi-Step Forecasting

The Rolling Mechanism (RM), which inspired the metabolic technique that updates the input data by discarding old data for each loop in the BP neural network, can be applied to perform the forecasting. The Rolling Mechanism forecasting steps are shown below.

- (a) 1-step ahead forecasting: The forecasting value $x_{N+1}^{forecast}$ is calculated based on the historical values, where N is the sample of training.
- (b) 2-step ahead forecasting: The forecasting value is $x_{N+2}^{forecast}$ calculated based on the historical values and the previous forecasting value $x_{N+1}^{forecast}$.
- (c) 3-step ahead forecasting: The forecasting value $x_{N+3}^{forecast}$ is calculated based on the historical values and the previous forecasting value $\{x_{N+1}^{forecast}, x_{N+2}^{forecast}\}$.

2.5. Adaptive Particle Swarm Optimization

An adaptive particle swarm optimization (APSO) is presented that features better search efficiency than classical particle swarm optimization (PSO). More importantly, it can perform a global search over the entire search space with a faster convergence speed. The APSO consists of two main steps. First, by evaluating the population distribution and particle fitness, a real-time evolutionary state estimation procedure is performed to identify one of four defined evolutionary states in each generation; exploration, exploitation, convergence, jumping out. It enables the automatic control of the inertia weight, acceleration coefficients, other algorithmic parameters at run time in order to improve the search efficiency and convergence speed. Then, an elitist learning strategy is performed when the evolutionary state is classified as the convergence state. This strategy will act on the globally best particle to jump out of the likely local optima [35].

3. Back Propagation Neural Network Optimized by Hybrid Optimization Algorithm

In order to optimize the initial weights and thresholds of the BP neural network, a novel APSOACO algorithm is introduced in this section.

3.1. Modified Ant Colony Optimization

The proposed APSOACO was inspired from the velocity update nature of particles from the adaptive particle swarm algorithm [35] and the foraging behavior of the ant colony algorithm [36,37]. We combine the distance metric of the ant colony algorithm with the direction (velocity) metric of the adaptive particle swarm algorithm and generate a new probability metric. The concept of the pheromone update in the ant colony algorithm is replaced with the velocity update from the particle swarm algorithm. A sigmoid function is used to convert distance and velocity into heuristic values. These heuristic values are used in the probability metric with different weights (shown in Section 4). The advantages of the hybrid algorithm include: (1) avoiding convergence to a local optimum; (2) providing a better solution within fewer iterations (fast convergence) and (3) achieving low computational complexity. In APSOACO, we denote the swarm population as particles (as ‘ants’ in the ant colony algorithm and ‘particles’ in the adaptive particle swarm algorithm). The basic steps of the APSOACO algorithm are presented as follows:

Step 1: Initialize a certain number of three-dimensional particle swarms P_0, P_1, \dots, P_n randomly.

Step 2: Feed the parameters corresponding to each particle back into the ant colony algorithm. Each particle corresponds to a set of parameters (α, β, ρ) . Apply this group of parameters to the ant colony algorithm, then reinitialize the pheromone in the environment. According to the resulting solution, update the pheromone. The ant colony algorithm adopts the pheromone update method combined with the global asynchronous and elitist strategy, which does not change the pheromone with an increasing number of ant colony algorithm iterations. If a more adaptive solution appears, the pheromone is updated and the path of the global optimal solution is enhanced. The pheromone updating formula is as follows:

$$\Delta\tau'_{ij}(t) = \begin{cases} Q/G_k & \text{if } [i, j] \text{ is the min error} \\ 0 & \text{otherwise} \end{cases}$$

where τ'_{ij} represents the amount of pheromone released by the best ant with the minimum error. Q is the total amount of pheromone; G_k is the minimum error; and ρ is the degree of volatilization of the pheromones. The range of values is $[0,1]$; τ_{ij1} is expressed as the update pheromone when it is updated by a basic updating mode and maintains the current algebra when stronger fitness is needed to solve the pheromone quantity. The calculation formula is as follows:

$$\tau_{ij1}(t+1) = (1-\rho)\tau_{ij1}(t) + \Delta\tau_{ij1}(t)$$

$$\Delta\tau_{ij1}(t) = \sum \tau_{ij}^k(t)$$

where $\Delta\tau_{ij1}$ is the released amount of pheromone with the error $[i, j]$ by the k th ant in this cycle and $\Delta\tau_{ij1}$ is the change of the τ_{ij1} on the error $[i, j]$ after this cycle. In the ant-cycle model, the formula of $\Delta\tau_{ij1}$ is as follows:

$$\Delta\tau_{ij1}(t) = \begin{cases} Q/L_k & \text{the } k\text{th pass the error } [i, j] \\ 0 & \text{otherwise} \end{cases}$$

where L_k is the error obtained by the k th ant in this cycle. In this step the pheromones are not cleared when the particles and their corresponding parameters are changed.

Step 3: According to the results of ant colony algorithm in judging the location of particles, find and update the optimal particle position. If the corresponding parameters of a particle are returned to the ant colony algorithm, the ant colony algorithm can obtain the best solution, so it calls this particle the optimal particle. A set of corresponding parameters of the optimal particle indicates the location of the particle in the solution space; that is, the best particle position. The location of the optimal particle is P_{best} . The optimal particle location found in the whole population is G_{best} . The fitness values of G_{best}

and P_{best} are used to evaluate the error of the ant colony algorithm—the smaller the error, the better the quality of the parameters.

Step 4: Update the position and velocity of the particle according to the following equations:

$$V_i(k+1) = \omega(k)V_i(k) + c_1r_1(P_{best,i} - x_i(k)) + c_2r_2(G_{best} - x_i(k))$$

$$x_i(k+1) = x_i(k) + V_i(k+1)$$

$$\omega(k+1) = \begin{cases} \lambda\omega(k) + \theta \frac{f(G_{best}) - f(x_i(k))}{f(G_{best}) - f(x_{min}(k))} & \omega(k) > \omega_{min} \\ \omega_{min} & \text{otherwise} \end{cases}$$

where $\omega(k)$ is the adaptive inertia weight, c_1 is the weight that makes the particle move to its own best position. c_2 is the weight that makes the particle move to the global best position. The range of c_1 and c_2 is $[0,2]$. r_1 and r_2 are two independent random numbers in the range of $0-1$; λ and θ are constraint factors in the range of $0-1$; ω_{min} is the minimum inertia weight; $f(\cdot)$ is the fitness function; $V_i(k)$ is the velocity of particle i at iteration k ; $x_i(k)$ is the position of particle i at the iteration; $P_{best,i}$ is the current best local position of particle i at iteration k . G_{best} is the global best solution of all particles.

Step 5: If the stopping criteria is satisfied (by arriving at the maximum number of iterations or particles to achieve the minimum goal value), the algorithm will stop and return to the current global optimum particle position. (α, β, ρ) is the best parameter combination in the ant colony algorithm. Otherwise, return to Step 2.

When optimizing the parameters (α, β, ρ) of the ant colony algorithm by applying the particle swarm optimization algorithm, introducing some new parameters (such as $\omega(k)$, c_1 , c_2 and maximum iteration) is unavoidable. The selection of the four parameters requires a certain level of experience, however the determination of their values is relatively simple and has only a small effect on the final solution. The ant colony algorithm will be completely called one time if the particle moves one time. Therefore, if the number of particle is N and they move M times, the ant colony algorithm will be called $N \times M$ times. Each time, the ant colony algorithm will iterate dozens or even hundreds of times.

3.2. Three Different Heuristic Algorithms for Optimizing BP Neural Network

In this section, the adaptive particle swarm algorithm, ant colony algorithm and APSOACO are applied to optimize the weights and the thresholds of the nonlinear BP neural network model by minimizing the mean square error of the BP neural network. However, the structure of the network is confirmed and, in order to achieve optimal parameters of the network, the fitness function and encoding strategy should be explained.

The purpose of the forecasting model is to minimize the mean square error of the BP neural network. According to Equation (21), the fitness value of the i th sample can be calculated as follows:

$$Fitness(X_i) = MSE(X_i)$$

The final step is to arrange the weights and the thresholds of the nonlinear BP network for each ant. In this paper, the structure of the weights and the thresholds matrix in the BP neural network is as follows:

$$Optimization\ matrix = [w_{ji}, w_{oj}]$$

where w_{ji} represents the connection weight from input node i to hidden node j . w_{oj} represents the connection threshold from hidden node j to the output node. Figure 1 shows the structures of the three different hybrid models.

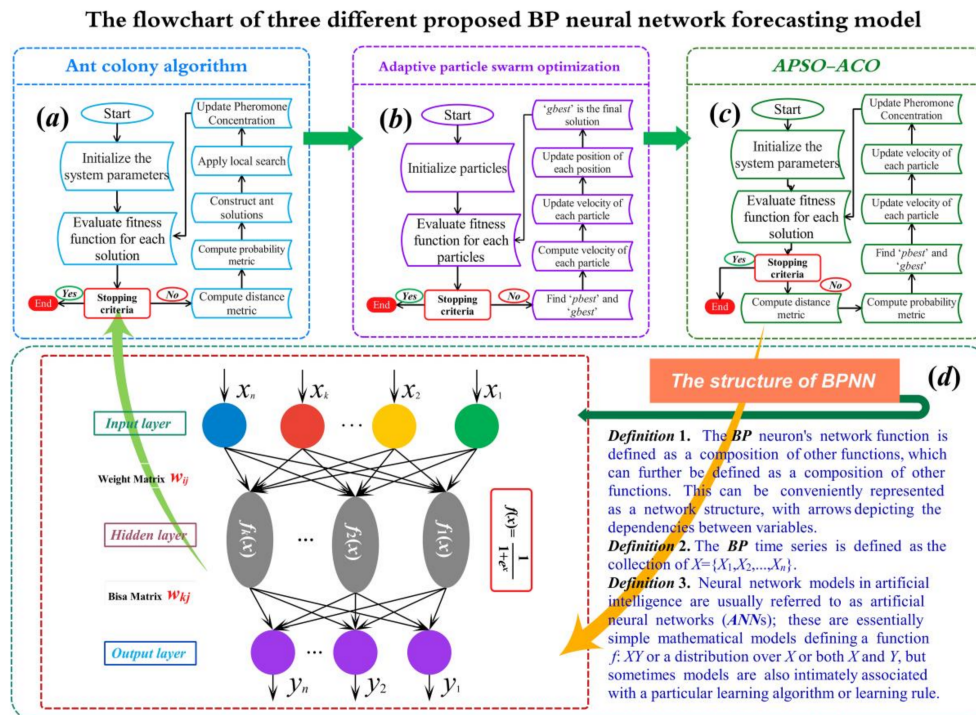


Figure 1. The structure of three different hybrid models. (a) the structure of neural network combined with ant colony optimization algorithm (b) the structure of neural network combined with adaptive particle swarm optimization algorithm. (c) the structure of neural network combined with hybrid optimization algorithm (d) the structure of neural network

4. Simulation Experimentation and Forecasting Result

In this study, 10 min ahead wind speed data from January 2014 from six study sites in the Shandong province of China were collected are employed to evaluate the effectiveness of this proposed integrated method. In order to further improve the wind speed forecasting performance, longitudinal data selection will be applied to construct the forecasting dataset.

4.1. Study Area and Data Description

Wind power generation turns the kinetic energy of wind into mechanical energy the mechanical energy is then transformed into electric energy. Wind speed plays a key role in this process. To verify the effectiveness of the proposed model, wind speed data from six observation sites were collected. Shandong is located in the east of China and has high level of wind activity every year. The long-term and stable distribution of wind power in the Shandong province is provided by onshore wind farms. The main types of turbines in the Shandong province are listed in Table 1. The speed in this area reaches 3 m/s more than 70% of the time, resulting in a good level of electricity generation. Table 2 shows the average monthly power generation distribution, where it is indicated that the distribution from January to July has a seasonal impact. The cut-in speed reaches approximately 70–80%. It is noted that in August the rated wind speed declines from 22% to 7%, the primary reason for which is strong tropical cyclone activity in the summer (which is harmful for turbines). Thus, there are some days when the wind farms cannot generate electricity in August.

According to the features of wind speed, six observation sites are used for this case study. However, the wind speed time series is not continuous in some months and has a number of missing data points. Specifically, for the six sites in Shandong, the number of missing data entries is 4464/48, 4464/54, 4464/66, 4464/32, 4464/18, 4464/96, respectively. We used fractal interpolation to deal with the missing data in this study [38].

Table 2. The main type of wind power turbines in Shandong province of China.

| Type Parameter | Guodian-UP82 | CCWE-1500/82.DF | Gamesa-G58/850 | Goldwind-GW82/1500 |
|---------------------|---------------------|---------------------|---------------------|---------------------|
| Rated power | 1500 KW | 1500 KW | 850 KW | 1500 KW |
| Cut-in Speed | 3 m/s | 3 m/s | 3 m/s | 3 m/s |
| Rated wind speed | 10.5 m/s | 11 m/s | 10.5 m/s | 10.3 m/s |
| Cut-out Speed | 25 m/s | 25 m/s | 22 m/s | 22 m/s |
| Survival wind speed | 52.5 m/s (3 s) |
| Swept area of rotor | 5384 m ² | 5278 m ² | 2642 m ² | 5324 m ² |
| Rotor diameter | 82.76 m | 82 m | 58 m | 82 m |

4.2. Evaluation Criteria of Forecasting Performance

To evaluate the forecasting performance, four forecasting error measures between the actual values and the forecasting values were employed for model evaluation and comparison: the average error (AE), mean absolute error (MAE), mean square error (MSE), mean absolute percentage error (MAPE) [37,38]. The smaller the values of these measures, the better the forecasting performance obtained. The definitions of these criteria can be indicated as follows.

$$AE = \frac{1}{N} \sum_{i=1}^N (x_i - \hat{x}_i).$$

$$MAE = \frac{1}{N} \sum_{i=1}^N |x_i - \hat{x}_i|.$$

$$MSE = \frac{1}{N} \sum_{i=1}^N (x_i - \hat{x}_i)^2.$$

$$MAPE = \frac{1}{N} \sum_{i=1}^N \left| \frac{x_i - \hat{x}_i}{x_i} \right| \times 100\%.$$

4.3. Experimental Process

To effectively forecast the wind speed, three forecasting experiments are implemented in this study. *Experiment I* aimed to compare the performance of different single artificial neural network models in order to select an individual model with the best performance among well-known forecasting models, with the best structure of each neural network for wind speed forecasting at each site. *Experiment II* was employed to compare the performances of the BP neural network when its parameters have been optimized by different optimization algorithms. *Experiment III* analyzed the forecasting performance offered by the proposed hybrid model in terms of multi-step ahead forecasting.

All the named algorithms were run on the platform 3.2 GHz CPU, 8.00 GB RAM, Windows 8, MATLAB R2012a. These experiments all selected from six wind speed data sites, which were described in Section 4.1. To evaluate the applicability, superiority, generality of the proposed novel combined model, wind speed data with a 10 min period from three datasets in Penglai, on the Shandong peninsula of China, were randomly assembled for multistep ahead forecasting (i.e., 1-step ahead, 2-step ahead, 3-step ahead). A large number of data points (2016) were selected from each dataset and these observations were split into two subsets; the training set and the testing set. In this paper, the experience proportion between the training and testing sets is 7:1. That is, the 1008 initial data points act as the training sample and the remaining 144 data points act as the testing sample and are repeated 7 times. In other words, in each of the wind speed data sites, the first 1008 data points are used as the training sample set and the next 1008 data points (from the 1009th to the 2016th) are used as the testing set.

4.4. The Experiment Preparation: Data Preprocessing

In order to enhance the prediction precision of the wind speed forecasting model, a valid mathematical data pre-processing module based on the theory of signal time-frequency localization was adopted. In this study, the Daubechies wavelet filter of order 4 (db4) decomposed the wind speed time series 7 levels and reconstituted the time series for each of the sites. For more detailed

information about wavelet transforms and wavelet de-noising techniques, please refer to the research by Authors [39–41].

4.5. Structure of the Proposed Forecasting Framework

At the beginning of this paper, fractal interpolation was used to estimate missing values of the original wind speed time series. Then, the wavelet de-noising method was used to pre-process the original time series. However, the wavelet de-noising need to select two parameters: the wavelet function and the number of decomposition level. In this, the wavelet function is Daubechies and the level is 7.

After the data pre-processing, the de-noised wind speed time series data was input into the optimized neural network, in which the parameter of neural network were optimized by three different optimization algorithms (APSO, ACO, APSOACO). The flowchart of the proposed model is shown in Figure 1.

It is worth pointing out that the original wind speed time series is divided into a training set and a testing set, which means the input data of the training data and testing data is de-noising data and the output data of the training data and testing data is the original wind speed time series. The flowchart of data structures of the forecasting models is shown in Figure 2.

For the Figure 2, N is the number of the training sample which is fixed according to the original time series. For example, supposing a study the last 1008 points of the wind speed time series with length of 2016 ($N = 1008$) will be forecasted.

It must be noting that there are multi-step ahead forecasting $h = 1, 2, 3$ of different wind speed sites in this paper.

4.6. Experiment I: Selection of the Wind Speed Forecasting Model

There are some artificial intelligence algorithms, such as the BP NN, the Elman NN, WNN, GRNN, ELM, that can be used to forecast the wind speed. The artificial intelligence forecasting models used in different forecasting steps in this experiment and the flowchart of the experiment are shown in Figure 2 and the experimental results follow in a later section.

To determine the number of neurons many experiments were conducted the best trial results were selected [42,43]. In this experiment, the listing technique was used to determine the number of input layers and hidden layers for the different ANN models [44]. From Figure 3 and Table 3, the following conclusions were obtained:

- (1) Table 3 shows the range of the input layer of each neural network is 3–8. With an increasing number of hidden layers, the test accuracy is gradually improved. When the number of hidden layers reaches a certain maximum number, the test accuracy is no longer improved.
- (2) Figure 3B shows that with an increase in the number included in the training sample, the fluctuation of testing accuracy reduces. For example, the confidence intervals obtained by the MAPE of the BP neural network is narrower than in the other four kinds of neural networks.

From the above analysis, it can be seen that the best performance for all sites (shown in Figure 4) among the five different neural networks is offered by the Back-propagation Neural Network.

Remark 1. *Through the above-mentioned analysis, we discovered that it is hard to find the general relationship between the nodes of the input layer and the hidden layer. Different time series have different forecasting structures, which suggests that different time series need to construct different BP neural networks structures. The best forecasting structure of the neural network is obtained by the enumeration method and experimental results.*

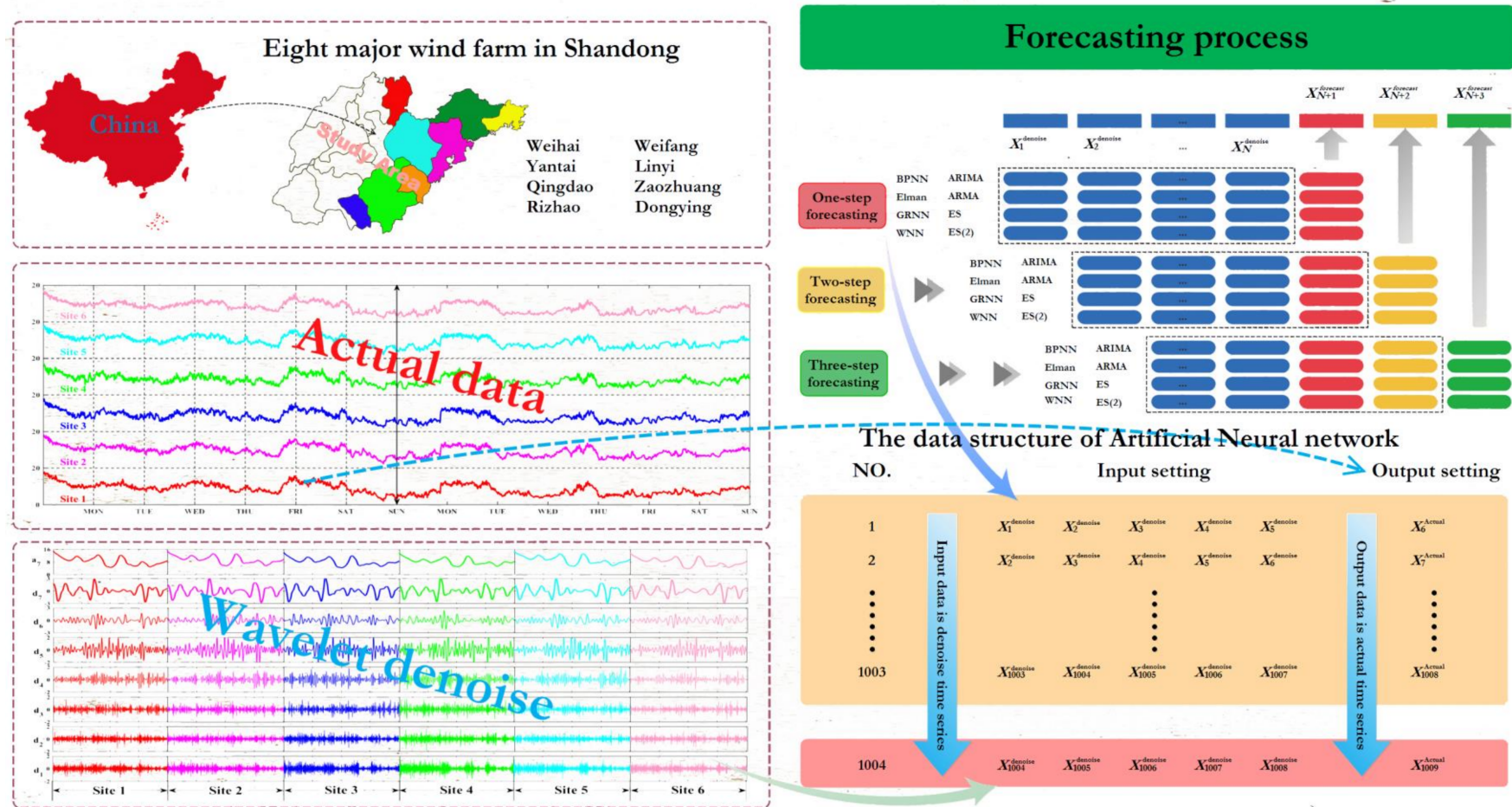
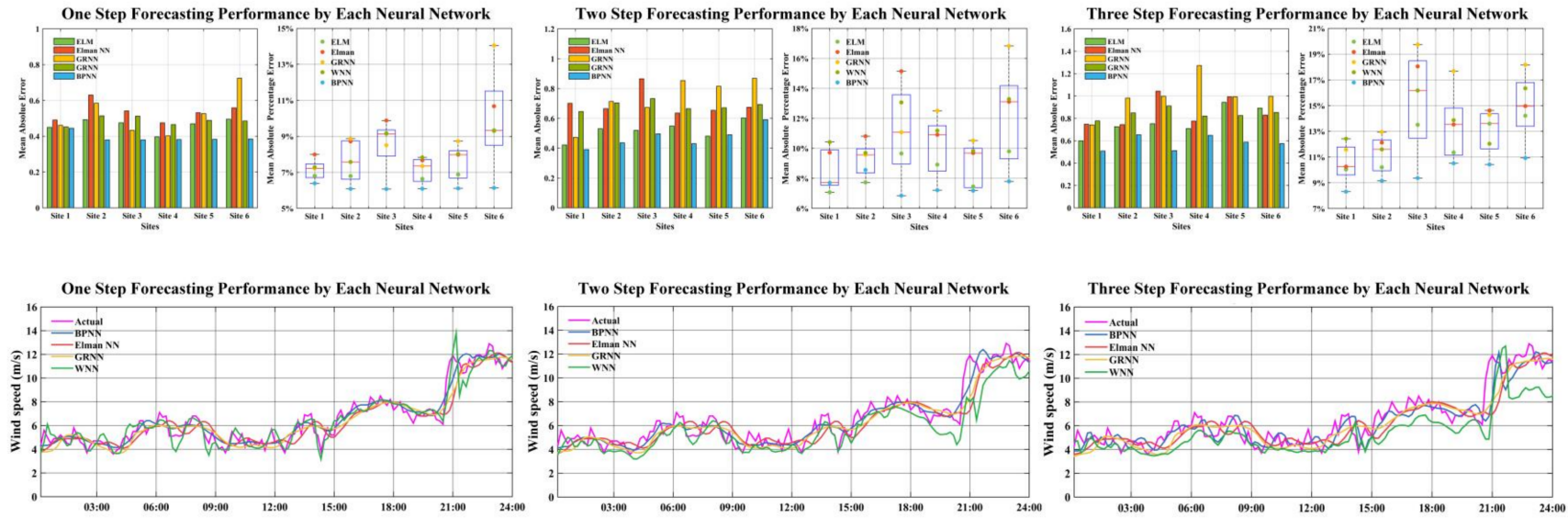


Figure 2. The data structures of the forecasting process (the six wind speed time series were generated in the Shandong province. The actual data was pre-processed by a wavelet de-noise. In the forecasting process, the training sample numbers 1008, the output sample numbers 144. The input data is the de-noised time series and the output data is the actual time series).

Part A: The Forecasting performance by Each ANN Model for Multi-step ahead Forecasting



Part B: The Forecasting Accuracy by Each Model with Different Training Sample and Different Hidden Layer

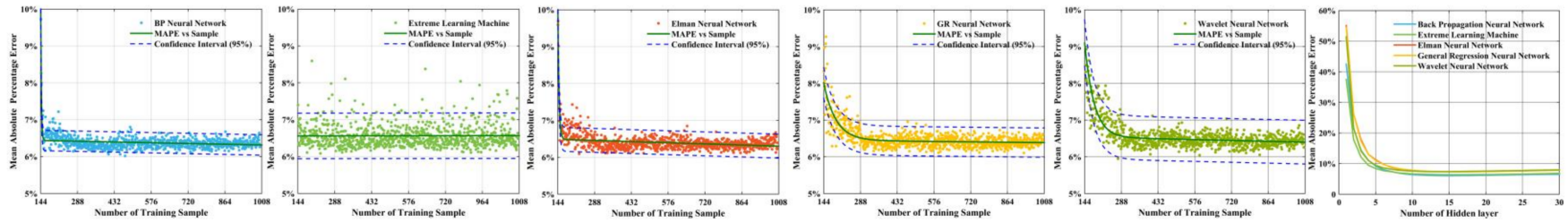


Figure 3. Forecasting performance by each neural network.

Table 3. Forecasting result by different Artificial Neural Network and the best forecasting structure.

| Forecasting Step | | One-Step Forecasting | | | | | | Two-Step Forecasting | | | | | | Three-Step Forecasting | | | | | |
|------------------|--------|----------------------|--------|--------|--------|--------|--------|----------------------|--------|--------|--------|--------|--------|------------------------|--------|--------|--------|--------|--------|
| Model | Metric | Site 1 | Site 2 | Site 3 | Site 4 | Site 5 | Site 6 | Site 1 | Site 2 | Site 3 | Site 4 | Site 5 | Site 6 | Site1 | Site 2 | Site 3 | Site 4 | Site 5 | Site 6 |
| BPNN | Input | 6 | 5 | 5 | 4 | 5 | 5 | 5 | 8 | 6 | 4 | 8 | 8 | 7 | 7 | 5 | 4 | 5 | 5 |
| | Hidden | 14 | 18 | 16 | 17 | 15 | 14 | 15 | 13 | 14 | 15 | 17 | 14 | 15 | 16 | 12 | 14 | 19 | 12 |
| | MAE | 0.4451 | 0.3798 | 0.3799 | 0.3817 | 0.3828 | 0.3851 | 0.3912 | 0.4360 | 0.4962 | 0.4303 | 0.4902 | 0.5915 | 0.5080 | 0.6535 | 0.5114 | 0.6485 | 0.5872 | 0.5746 |
| | MSE | 0.3504 | 0.2315 | 0.2327 | 0.2356 | 0.2374 | 0.2418 | 0.3051 | 0.2858 | 0.3717 | 0.3469 | 0.2789 | 0.3249 | 0.3822 | 0.5174 | 0.3887 | 0.3962 | 0.4139 | 0.4504 |
| | MAPE | 6.39% | 6.08% | 6.07% | 6.09% | 6.11% | 6.14% | 7.71% | 8.56% | 6.85% | 7.21% | 7.18% | 7.80% | 8.31% | 9.16% | 9.36% | 10.51% | 10.42% | 10.93% |
| ELM | Input | 5 | 6 | 3 | 3 | 6 | 7 | 7 | 8 | 3 | 5 | 4 | 7 | 7 | 3 | 3 | 4 | 6 | 7 |
| | Hidden | 17 | 14 | 18 | 14 | 16 | 18 | 18 | 24 | 14 | 15 | 14 | 13 | 21 | 18 | 19 | 16 | 22 | 14 |
| | MAE | 0.45 | 0.4927 | 0.4751 | 0.3966 | 0.4696 | 0.4952 | 0.4215 | 0.5302 | 0.5196 | 0.5486 | 0.4809 | 0.6023 | 0.5995 | 0.7258 | 0.752 | 0.7086 | 0.9431 | 0.8917 |
| | MSE | 0.3661 | 0.4056 | 0.3583 | 0.2305 | 0.3787 | 0.477 | 0.3059 | 0.4283 | 0.4886 | 0.5111 | 0.3606 | 0.926 | 0.6654 | 0.9146 | 1.0531 | 0.9368 | 1.5351 | 1.4202 |
| | MAPE | 6.81% | 6.79% | 9.18% | 6.64% | 6.88% | 9.34% | 7.07% | 7.73% | 9.66% | 8.91% | 7.45% | 9.80% | 10.04% | 10.20% | 13.50% | 11.35% | 13.60% | 14.21% |
| Elman NN | Input | 8 | 3 | 6 | 5 | 3 | 5 | 8 | 6 | 6 | 3 | 8 | 6 | 7 | 4 | 5 | 6 | 7 | 3 |
| | Hidden | 19 | 14 | 19 | 14 | 20 | 15 | 16 | 19 | 17 | 13 | 15 | 13 | 25 | 22 | 18 | 18 | 18 | 16 |
| | MAE | 0.4907 | 0.6304 | 0.5416 | 0.4751 | 0.5313 | 0.5588 | 0.701 | 0.6651 | 0.8654 | 0.6358 | 0.6538 | 0.6746 | 0.7477 | 0.7442 | 1.0435 | 0.7758 | 0.9926 | 0.8299 |
| | MSE | 0.4137 | 0.6411 | 0.5779 | 0.392 | 0.4807 | 0.5817 | 0.7878 | 0.7737 | 1.3138 | 0.7216 | 0.6604 | 0.8593 | 0.9062 | 0.9775 | 1.9776 | 1.1036 | 1.4048 | 1.2713 |
| | MAPE | 7.99% | 8.72% | 9.88% | 7.67% | 7.98% | 10.67% | 9.72% | 10.81% | 15.14% | 10.91% | 9.69% | 13.11% | 10.26% | 12.13% | 18.05% | 13.53% | 14.62% | 14.96% |
| GRNN | Input | 3 | 7 | 4 | 6 | 3 | 6 | 4 | 4 | 5 | 3 | 8 | 8 | 6 | 6 | 7 | 7 | 6 | 5 |
| | Hidden | 13 | 14 | 17 | 16 | 15 | 19 | 18 | 18 | 16 | 24 | 17 | 13 | 23 | 19 | 16 | 25 | 24 | 19 |
| | MAE | 0.4609 | 0.5847 | 0.4332 | 0.4018 | 0.5263 | 0.7246 | 0.4726 | 0.713 | 0.6729 | 0.8537 | 0.8151 | 0.8687 | 0.7418 | 0.9813 | 0.9974 | 1.2723 | 0.9933 | 0.9972 |
| | MSE | 0.3429 | 0.5522 | 0.287 | 0.2851 | 0.4496 | 0.9465 | 0.3791 | 0.9494 | 1.2302 | 1.3197 | 1.2783 | 1.3276 | 1.0239 | 1.6089 | 1.7512 | 2.74 | 1.6364 | 1.8682 |
| | MAPE | 7.22% | 8.87% | 8.51% | 7.35% | 8.73% | 14.05% | 7.71% | 9.57% | 11.07% | 12.51% | 10.52% | 16.83% | 11.57% | 12.95% | 19.75% | 17.68% | 14.28% | 18.17% |
| WNN | Input | 4 | 6 | 7 | 7 | 5 | 3 | 7 | 5 | 4 | 5 | 3 | 3 | 6 | 6 | 4 | 4 | 5 | 4 |
| | Hidden | 17 | 16 | 20 | 14 | 18 | 18 | 25 | 25 | 20 | 12 | 15 | 16 | 23 | 14 | 15 | 14 | 15 | 18 |
| | MAE | 0.4521 | 0.514 | 0.5126 | 0.4652 | 0.489 | 0.4854 | 0.6458 | 0.7038 | 0.7323 | 0.6646 | 0.6708 | 0.6934 | 0.7772 | 0.8486 | 0.9113 | 0.8207 | 0.8252 | 0.8531 |
| | MSE | 0.3821 | 0.4354 | 0.4842 | 0.3599 | 0.4219 | 0.4239 | 0.7797 | 0.8277 | 0.9881 | 0.7345 | 0.7729 | 0.865 | 1.1074 | 1.2171 | 1.4874 | 1.112 | 1.145 | 1.2837 |
| | MAPE | 7.29% | 7.58% | 9.14% | 7.83% | 8.03% | 9.30% | 10.42% | 9.70% | 13.06% | 11.18% | 9.83% | 13.29% | 12.42% | 11.60% | 16.18% | 13.86% | 12.04% | 16.34% |

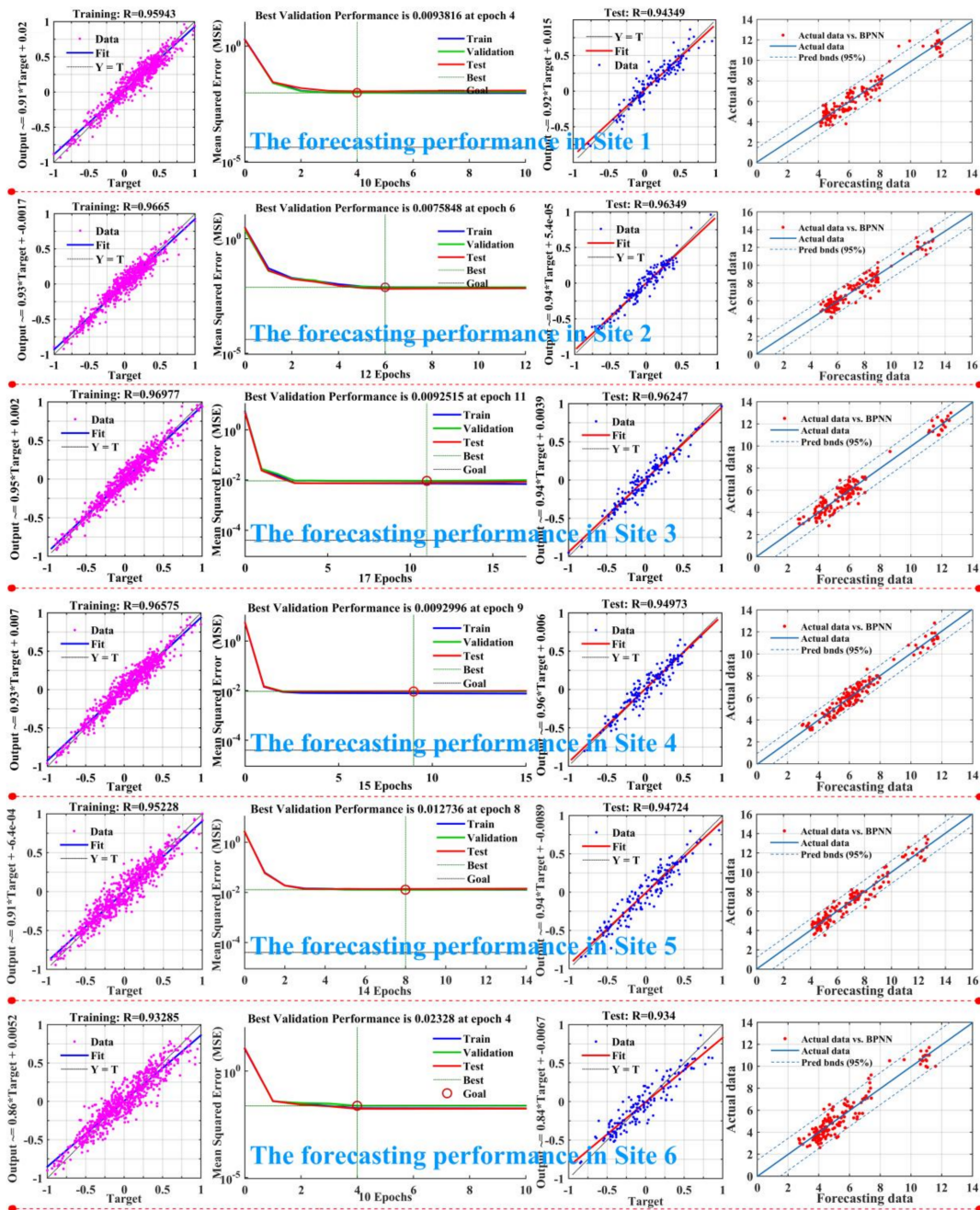


Figure 4. Best structure of BPNN for prediction result in each site.

4.7. Experiment II: Comparison of Three Optimization Algorithms to Fine-Tune the Parameters of Hybrid Model

In order to evaluate the forecasting performance of the hybrid model optimized by three different optimization algorithms (two traditional algorithms and APSOACO), three different optimization algorithms are used to optimize the hidden layer and output layer weight matrix the neural network and to optimize hidden layer and output layer parameter matrix. Two other measures (the Index Agreement and *Bias*²) are also employed for model evaluation.

The Index Agreement is a dimensionless index that measures the fitness of the model, ranging from 0 (worst fitness) to 1 (best fitness) [45].

$$IA = 1 - \frac{\sum_{i=1}^T (x_i - \hat{x}_i)^2}{\sum_{i=1}^T (|x_i - \hat{x}_i| + |x_i - \bar{x}|)^2}$$

\hat{x}_i and x_i are the forecasting and actual values of wind speed at time point i of the forecasting horizon T , respectively. \bar{x} is the mean of the actual values of the wind speed.

$$VAR(\hat{x}) + Bias^2(\hat{x}) = E[\hat{x} - E(\hat{x})]^2 + [x - E(\hat{x})]^2$$

x_i is the actual data, \hat{x}_i is the forecasting data, $E(\hat{x}) = \frac{1}{N} \sum_{i=1}^N \hat{x}_i$ is the expectation value of the forecasting data, $x = \frac{1}{N} \sum_{i=1}^N x_i$ is the expectation of the actual data. N is the number of the sample. The bias-variance framework [46] is employed to evaluate the forecasting accuracy and stability of the forecasting models. In this framework, the values of $Bias^2(\hat{x})$ and $VAR(\hat{x})$ reflect the accuracy and stability of the forecasting model, respectively.

10 min wind speed time series were generated from 5–18 January at each site. Figure 5 shows the data structures of the forecasting models involved in this paper. For instance, the total sample size is 2016, data of the former seven days (sample size 1008) are the training sample. The remaining data are the testing sample. The input of this proposed hybrid model is set as the de-noised wind speed time series data, which is shown in Figure 2. This is achieved by employing the wavelet function decomposed (the wavelet is Daubechies (db4) and the decomposition level is 7) to the wind speed series. The final assessment of the 1-step ahead forecasting results is shown in Table 4.

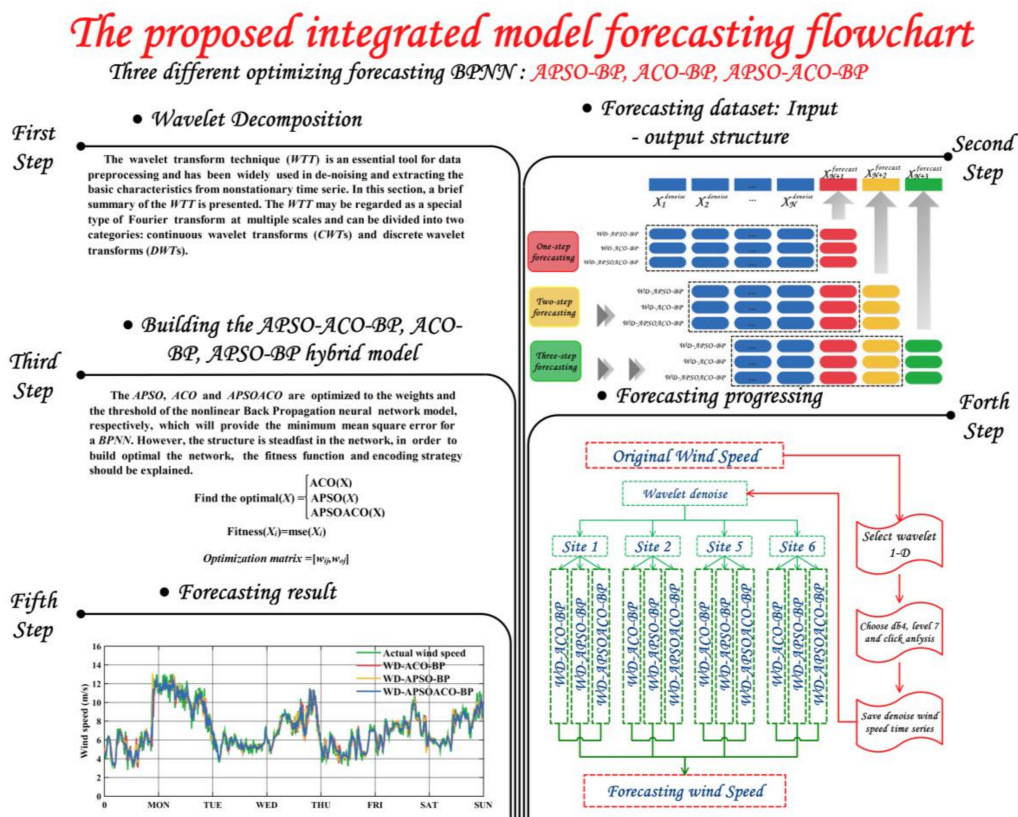


Figure 5. Flowchart of three hybrid forecasting models.

Table 4. The forecasting result of each site (1-step forecasting).

| Forecasting Model | Metric | Site | | | | | |
|-------------------|-------------------|---------------|---------------|---------------|---------------|---------------|---------------|
| | | Site 1 | Site 2 | Site 3 | Site 4 | Site 5 | Site 6 |
| WD-GRNN | MAE | 0.3922 | 0.4123 | 0.4102 | 0.4220 | 0.4139 | 0.4193 |
| WD-Elman | | 0.4039 | 0.4141 | 0.3913 | 0.3981 | 0.3948 | 0.4219 |
| WD-BP | | 0.4022 | 0.3956 | 0.3896 | 0.4075 | 0.4045 | 0.4061 |
| WD-WNN | | 0.4099 | 0.4112 | 0.4042 | 0.3936 | 0.4119 | 0.3903 |
| WD-APSO-BP | | 0.3850 | 0.3886 | 0.4272 | 0.4470 | 0.3985 | 0.3818 |
| WD-ACO-BP | | 0.3913 | 0.4123 | 0.4388 | 0.4904 | 0.4179 | 0.4025 |
| WD-APSOACO-BP | | 0.3027 | 0.3129 | 0.3446 | 0.3535 | 0.3225 | 0.3108 |
| WD-GRNN | MSE | 0.2499 | 0.2603 | 0.3405 | 0.3870 | 0.2857 | 0.2811 |
| WD-Elman | | 0.2573 | 0.2614 | 0.3248 | 0.3651 | 0.2725 | 0.2829 |
| WD-BP | | 0.2562 | 0.2498 | 0.3234 | 0.3738 | 0.2791 | 0.2722 |
| WD-WNN | | 0.2612 | 0.2596 | 0.3355 | 0.3610 | 0.2843 | 0.2617 |
| WD-APSO-BP | | 0.2453 | 0.2431 | 0.3196 | 0.3531 | 0.2657 | 0.2581 |
| WD-ACO-BP | | 0.2503 | 0.4520 | 0.3408 | 0.4159 | 0.3105 | 0.2972 |
| WD-APSOACO-BP | | 0.1528 | 0.1618 | 0.2163 | 0.2239 | 0.1759 | 0.1753 |
| WD-GRNN | MAPE | 5.96% | 5.39% | 6.71% | 6.85% | 5.62% | 6.97% |
| WD-Elman | | 6.13% | 5.41% | 6.40% | 6.46% | 5.36% | 7.02% |
| WD-BP | | 6.11% | 5.17% | 6.37% | 6.61% | 5.49% | 6.75% |
| WD-WNN | | 6.23% | 5.37% | 6.61% | 6.39% | 5.59% | 6.49% |
| WD-APSO-BP | | 5.85% | 5.03% | 6.30% | 6.25% | 5.22% | 6.40% |
| WD-ACO-BP | | 5.93% | 5.28% | 6.47% | 6.88% | 5.48% | 6.72% |
| WD-APSOACO-BP | | 4.59% | 4.05% | 5.02% | 4.89% | 4.21% | 5.23% |
| WD-GRNN | VAR(Y) | 0.8028 | 1.0009 | 0.8492 | 1.2014 | 0.9451 | 0.8391 |
| WD-Elman | | 0.8267 | 1.0051 | 0.8100 | 1.1335 | 0.9015 | 0.8444 |
| WD-BP | | 0.8232 | 0.9604 | 0.8065 | 1.1604 | 0.9236 | 0.8127 |
| WD-WNN | | 0.8390 | 0.9981 | 0.8367 | 1.1207 | 0.9406 | 0.7812 |
| WD-APSO-BP | | 0.7881 | 0.9346 | 0.7970 | 1.0962 | 0.8791 | 0.7705 |
| WD-ACO-BP | | 0.7654 | 1.1980 | 0.7964 | 1.0582 | 0.8832 | 0.8135 |
| WD-APSOACO-BP | | 0.7101 | 0.9090 | 0.7217 | 0.9192 | 0.8009 | 0.7405 |
| WD-GRNN | Bias ² | 1.5090 | 1.3165 | 1.3423 | 1.1463 | 1.2696 | 1.4001 |
| WD-Elman | | 1.5538 | 1.3221 | 1.2803 | 1.0815 | 1.2110 | 1.4089 |
| WD-BP | | 1.5473 | 1.2632 | 1.2748 | 1.1071 | 1.2406 | 1.3560 |
| WD-WNN | | 1.5770 | 1.3129 | 1.3226 | 1.0693 | 1.2635 | 1.3034 |
| WD-APSO-BP | | 1.4813 | 1.2293 | 1.2598 | 1.0459 | 1.1809 | 1.2856 |
| WD-ACO-BP | | 1.4668 | 1.1780 | 1.2961 | 1.0065 | 1.2866 | 1.4229 |
| WD-APSOACO-BP | | 1.4400 | 1.1852 | 1.2405 | 1.0029 | 1.1860 | 1.3891 |
| WD-GRNN | IA | 0.9443 | 0.8989 | 0.8875 | 0.8745 | 0.8878 | 0.8682 |
| WD-Elman | | 0.9170 | 0.8951 | 0.9305 | 0.9269 | 0.9308 | 0.8628 |
| WD-BP | | 0.9209 | 0.9368 | 0.9345 | 0.9054 | 0.9085 | 0.8965 |
| WD-WNN | | 0.9035 | 0.9014 | 0.9007 | 0.9374 | 0.8921 | 0.9327 |
| WD-APSO-BP | | 0.9398 | 0.9433 | 0.9196 | 0.9320 | 0.9299 | 0.9144 |
| WD-ACO-BP | | 0.9372 | 0.8943 | 0.9177 | 0.9232 | 0.9165 | 0.9109 |
| WD-APSOACO-BP | | 0.9619 | 0.9627 | 0.9456 | 0.9584 | 0.9545 | 0.9456 |

Note: Marked by bold is the best forecasting model.

- (1) It is noted that ACO suffers from slow convergence with increasing iterations. If the APSO algorithm falls into the local optimal points the capacity of the parameter optimization will be affected. The APSOACO algorithm combines the global search abilities of ACO with the local search capability of APSO, which significantly improves the parameter optimization ability of the single optimization algorithm. The numerical experimentation results indicate that the proposed hybrid model (WD-APSOACO-BP) outperforms the other hybrid models (WD-APSO-BP and WD-ACO-BP) when compared with the MAE, MSE, MAPE, the variance of MAPE, IA from Site 1 to Site 6. As such, the MAPE values of the WD-APSOACO-BP are 4.592%, 4.045%, 5.021%,

4.891%, 4.214%, 5.234%, corresponding to the $Bias^2$ values which are 1.4400, 1.1852, 1.2405, 1.0029, 1.1860 and 1.3891 from Site 1 to Site 6, respectively. The WD-APSOACO-BP model can obtain higher forecasting accuracy than two single hybrid models. However, the IA values are 0.9619, 0.9627, 0.9456, 0.9584, 0.9545, 0.9456 from Site 1 to Site 6, which demonstrates that the WD-APSOACO-BP can achieve a better forecasting performance than the other hybrid models. Thus, the WD-APSOACO-BP can precisely forecast the future changes of a wind speed time series.

- (2) With regards to further analysis of the forecasting results in terms of each day (the testing sample from Monday to Sunday), Table 5 and Figure 6A1–A4 clearly depict the forecasting values for 0:10 a.m. to 24:00 p.m., from 12 to 18. Part A and B of Figure 6 demonstrate the MAPE and IA from Site 1 to Site 6. The MAPE and IA of WD-APSOACO-BP are the minimum and the maximum, respectively. Part A1 of Figure 6 demonstrates the forecasting results of three different hybrid models and the actual wind speed series from 0:10 a.m. to 24:00 p.m., from 12 to 18 January 2014. Part A2 of Figure 6 demonstrates the 95% confidence intervals (CI) obtained by the WD-APSOACO-BP model. It can be clearly seen that both the upper CI and the lower CI are very close to the actual wind speed time series for Monday. Part A3 of Figure 6 is the Box-Plot of the MAPE from 0:10 a.m. to 24:00 p.m., over the course of a week, from 12–18 January, for the three hybrid models for Site 2. It can be seen that the performance of the WD-APSOACO-BP is better than that of the other two hybrid models. In addition, A4 clearly displays the actual wind speed time series compared with the forecasting results. It is obvious that the forecasting results offered by the proposed WD-APSOACO-BP method are very approximate to the target.

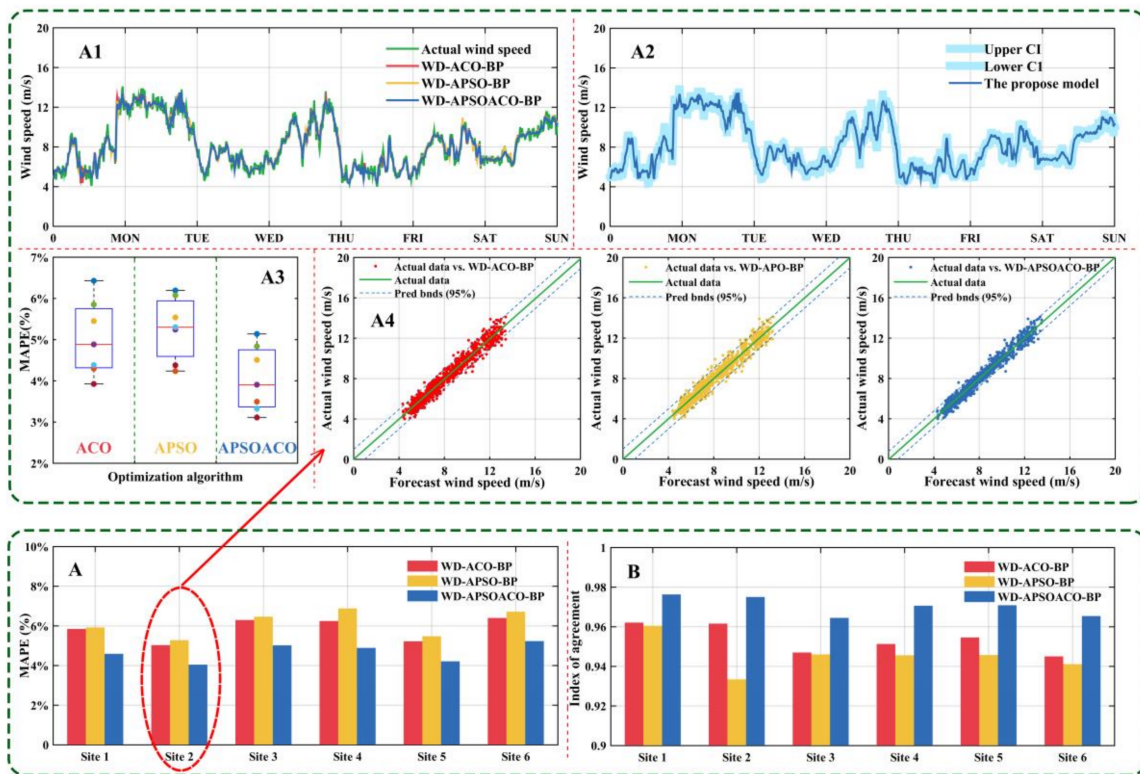


Figure 6. The forecasting results of three methods for Site 2 (1-step forecasting).

Table 5. The forecasting results of Site 2 (1-step forecasting).

| Week | Forecasting Model | Evaluation Criteria Metric | | | | | |
|------|-------------------|----------------------------|---------------|--------------|---------------|-------------------|---------------|
| | | MAE | MSE | MAPE | VAR(Y) | Bias ² | IA |
| MON | WD-GRNN | 0.4766 | 0.3352 | 7.05% | 1.5263 | 3.9215 | 0.9158 |
| | WD-Elman | 0.4806 | 0.3184 | 7.05% | 1.4606 | 4.1074 | 0.9723 |
| | WD-BP | 0.4463 | 0.3241 | 6.53% | 1.5045 | 4.0609 | 0.8994 |
| | WD-WNN | 0.4810 | 0.3325 | 7.05% | 1.4128 | 4.1238 | 0.8925 |
| | WD-APSO-BP | 0.4407 | 0.3153 | 6.43% | 1.3930 | 3.7628 | 0.9758 |
| | WD-ACO-BP | 0.4350 | 0.3243 | 6.20% | 1.2926 | 3.5912 | 0.9748 |
| | WD-APSOACO-BP | 0.3535 | 0.2156 | 5.14% | 1.1289 | 3.5740 | 0.9833 |
| Tue | WD-GRNN | 0.5350 | 0.4052 | 4.71% | 0.3503 | 1.1212 | 0.8379 |
| | WD-Elman | 0.5395 | 0.3848 | 4.71% | 0.3352 | 1.1743 | 0.8896 |
| | WD-BP | 0.5010 | 0.3917 | 4.36% | 0.3453 | 1.1611 | 0.8229 |
| | WD-WNN | 0.5399 | 0.4019 | 4.71% | 0.3242 | 1.1791 | 0.8166 |
| | WD-APSO-BP | 0.4947 | 0.3811 | 4.29% | 0.3197 | 1.0758 | 0.8928 |
| | WD-ACO-BP | 0.4889 | 0.3662 | 4.24% | 0.2824 | 1.0202 | 0.8902 |
| | WD-APSOACO-BP | 0.4045 | 0.2567 | 3.49% | 0.2770 | 0.9638 | 0.9302 |
| Wed | WD-GRNN | 0.3729 | 0.1864 | 5.97% | 0.6996 | 0.0295 | 0.8681 |
| | WD-Elman | 0.3760 | 0.1770 | 5.98% | 0.6695 | 0.0309 | 0.9216 |
| | WD-BP | 0.3492 | 0.1802 | 5.54% | 0.6896 | 0.0305 | 0.8525 |
| | WD-WNN | 0.3763 | 0.1849 | 5.98% | 0.6475 | 0.0310 | 0.8460 |
| | WD-APSO-BP | 0.3448 | 0.1753 | 5.45% | 0.6385 | 0.0283 | 0.9250 |
| | WD-ACO-BP | 0.3505 | 0.1828 | 5.54% | 0.6142 | 0.0311 | 0.9209 |
| | WD-APSOACO-BP | 0.2841 | 0.1193 | 4.51% | 0.5835 | 0.0222 | 0.9504 |
| Thu | WD-GRNN | 0.4860 | 0.3579 | 5.35% | 1.9743 | 1.2797 | 0.9029 |
| | WD-Elman | 0.4901 | 0.3399 | 5.35% | 1.8893 | 1.3403 | 0.9586 |
| | WD-BP | 0.4551 | 0.3460 | 4.96% | 1.9461 | 1.3252 | 0.8868 |
| | WD-WNN | 0.4904 | 0.3550 | 5.36% | 1.8274 | 1.3457 | 0.8799 |
| | WD-APSO-BP | 0.4494 | 0.3366 | 4.88% | 1.8019 | 1.2279 | 0.9621 |
| | WD-ACO-BP | 0.4836 | 0.3774 | 5.24% | 1.8477 | 1.1867 | 0.9576 |
| | WD-APSOACO-BP | 0.3629 | 0.2237 | 3.90% | 1.7010 | 1.1400 | 0.9754 |
| Fri | WD-GRNN | 0.3594 | 0.1792 | 6.41% | 0.4739 | 0.2404 | 0.8513 |
| | WD-Elman | 0.3624 | 0.1701 | 6.42% | 0.4535 | 0.2518 | 0.9038 |
| | WD-BP | 0.3365 | 0.1732 | 5.94% | 0.4671 | 0.2489 | 0.8360 |
| | WD-WNN | 0.3627 | 0.1777 | 6.42% | 0.4386 | 0.2528 | 0.8296 |
| | WD-APSO-BP | 0.3323 | 0.1685 | 5.85% | 0.4325 | 0.2307 | 0.9071 |
| | WD-ACO-BP | 0.3503 | 0.1930 | 6.08% | 0.3757 | 0.2170 | 0.8904 |
| | WD-APSOACO-BP | 0.2774 | 0.1195 | 4.84% | 0.3301 | 0.2033 | 0.9355 |
| Sat | WD-GRNN | 0.3906 | 0.1894 | 5.27% | 2.2004 | 0.3582 | 0.8230 |
| | WD-Elman | 0.3939 | 0.1798 | 5.27% | 2.1057 | 0.3752 | 0.8737 |
| | WD-BP | 0.3658 | 0.1831 | 4.89% | 2.1689 | 0.3709 | 0.8082 |
| | WD-WNN | 0.3942 | 0.1878 | 5.28% | 2.0367 | 0.3767 | 0.8020 |
| | WD-APSO-BP | 0.3612 | 0.1781 | 4.81% | 2.0082 | 0.3437 | 0.8769 |
| | WD-ACO-BP | 0.4206 | 1.5319 | 5.30% | 3.1669 | 0.0658 | 0.6492 |
| | WD-APSOACO-BP | 0.2507 | 0.0977 | 3.33% | 1.0815 | 0.2051 | 0.9764 |
| Sun | WD-GRNN | 0.3536 | 0.1659 | 4.30% | 0.9602 | 2.1656 | 0.9213 |
| | WD-Elman | 0.3566 | 0.1575 | 4.30% | 0.9189 | 2.2683 | 0.9782 |
| | WD-BP | 0.3312 | 0.1603 | 3.99% | 0.9465 | 2.2426 | 0.9048 |
| | WD-WNN | 0.3569 | 0.1645 | 4.30% | 0.8888 | 2.2774 | 0.8979 |
| | WD-APSO-BP | 0.3270 | 0.1560 | 3.92% | 0.8763 | 2.0780 | 0.9817 |
| | WD-ACO-BP | 0.3569 | 0.1884 | 4.38% | 0.8564 | 2.2791 | 0.9770 |
| | WD-APSOACO-BP | 0.2572 | 0.1001 | 3.11% | 0.8115 | 1.9563 | 0.9878 |

Note: Marked by bold is the best forecasting model.

Remark 2. The above experimental analysis aimed to demonstrate whether the MAE, MSE, VAR(Y), MAPE, Bias² and IA of the proposed WD-APSOACO-BP hybrid model mean it manifests the best forecasting performance. In brief, the proposed hybrid optimization algorithm has a better capacity for optimization to find the optimum weights and thresholds for the Nonlinear BP Neural Network.

4.8. Experiment III: Comparison Three Different Hybrid Models in Multi-Step Ahead Wind Speed Forecasting

To further verify the feasibility, performance, meliority of the proposed hybrid forecasting model, the wind speed data from six sites are employed for establishing the proposed WD-APSOACO-BP model. In addition, the proposed hybrid WD-APSOACO-BP model is compared with two other forecasting models (WD-APSO-BP and WD-ACO-BP) for multi-step ahead wind speed forecasting. The results are shown in Tables 6 and 7 and Figures 7 and 8. The index of agreement produced by the proposed hybrid model for the 2-step and 3-step ahead wind speed forecasts of different sites is shown in Part B of Figures 7 and 8.

Table 6. The forecasting result of each site (2-step forecasting).

| Forecasting Model | Metric | Site | | | | | |
|-------------------|-------------------|---------------|---------------|---------------|---------------|---------------|---------------|
| | | Site 1 | Site 2 | Site 3 | Site 4 | Site 5 | Site 6 |
| WD-GRNN | MAE | 0.4743 | 0.4707 | 0.5043 | 0.5565 | 0.4999 | 0.4446 |
| WD-Elman | | 0.4779 | 0.4493 | 0.493 | 0.5368 | 0.4972 | 0.4578 |
| WD-BP | | 0.4772 | 0.4729 | 0.4955 | 0.5697 | 0.5156 | 0.4558 |
| WD-WNN | | 0.4616 | 0.4431 | 0.5311 | 0.5221 | 0.517 | 0.4646 |
| WD-APSO-BP | | 0.4442 | 0.4417 | 0.4907 | 0.5203 | 0.4789 | 0.4364 |
| WD-ACO-BP | | 0.4631 | 0.4786 | 0.5249 | 0.5356 | 0.4879 | 0.4797 |
| WD-APSOACO-BP | | 0.3664 | 0.349 | 0.3954 | 0.4127 | 0.3802 | 0.3472 |
| WD-GRNN | | MSE | 0.3588 | 0.3625 | 0.4553 | 0.5006 | 0.423 |
| WD-Elman | 0.3615 | | 0.346 | 0.445 | 0.4829 | 0.4207 | 0.372 |
| WD-BP | 0.361 | | 0.3642 | 0.4473 | 0.5126 | 0.4362 | 0.3704 |
| WD-WNN | 0.3492 | | 0.3413 | 0.4795 | 0.4697 | 0.4374 | 0.3775 |
| WD-APSO-BP | 0.336 | | 0.3402 | 0.443 | 0.4681 | 0.4052 | 0.3546 |
| WD-ACO-BP | 0.3617 | | 0.4515 | 0.4927 | 0.4994 | 0.4073 | 0.4275 |
| WD-APSOACO-BP | 0.2309 | | 0.2135 | 0.2894 | 0.3041 | 0.2547 | 0.2298 |
| WD-GRNN | MAPE | | 0.0621 | 0.0707 | 0.075 | 0.0791 | 0.066 |
| WD-Elman | | 0.0626 | 0.0675 | 0.0733 | 0.0763 | 0.0656 | 0.0768 |
| WD-BP | | 0.0625 | 0.071 | 0.0737 | 0.081 | 0.068 | 0.0765 |
| WD-WNN | | 0.0605 | 0.0666 | 0.079 | 0.0742 | 0.0682 | 0.078 |
| WD-APSO-BP | | 5.82% | 6.63% | 7.30% | 7.39% | 6.32% | 7.33% |
| WD-ACO-BP | | 6.06% | 7.34% | 7.89% | 7.56% | 6.43% | 7.99% |
| WD-APSOACO-BP | | 4.79% | 5.25% | 5.90% | 5.87% | 5.07% | 5.79% |
| WD-GRNN | | VAR(Y) | 1.0272 | 0.8286 | 0.842 | 1.2089 | 0.9778 |
| WD-Elman | 1.0348 | | 0.7909 | 0.8231 | 1.1662 | 0.9724 | 0.8607 |
| WD-BP | 1.0334 | | 0.8325 | 0.8273 | 1.2378 | 1.0084 | 0.8571 |
| WD-WNN | 0.9996 | | 0.7801 | 0.8868 | 1.1343 | 1.0112 | 0.8735 |
| WD-APSO-BP | 0.9619 | | 0.7776 | 0.8193 | 1.1304 | 0.9367 | 0.8205 |
| WD-ACO-BP | 0.9618 | | 0.7818 | 0.8096 | 1.1296 | 0.8797 | 0.7911 |
| WD-APSOACO-BP | 0.9302 | | 0.7766 | 0.7862 | 1.0212 | 0.8679 | 0.7844 |
| WD-GRNN | Bias ² | | 1.2105 | 1.4909 | 1.2759 | 1.0236 | 1.219 |
| WD-Elman | | 1.2195 | 1.4232 | 1.2472 | 0.9874 | 1.2124 | 1.451 |
| WD-BP | | 1.2178 | 1.498 | 1.2536 | 1.048 | 1.2572 | 1.4449 |
| WD-WNN | | 1.1781 | 1.4037 | 1.3437 | 0.9604 | 1.2607 | 1.4727 |
| WD-APSO-BP | | 1.1336 | 1.3992 | 1.2415 | 0.9571 | 1.1678 | 1.3833 |
| WD-ACO-BP | | 1.1436 | 1.408 | 1.1462 | 0.9694 | 1.145 | 1.3562 |
| WD-APSOACO-BP | | 1.1183 | 1.3064 | 1.1245 | 0.9019 | 1.1295 | 1.3219 |
| WD-GRNN | | IA | 0.8634 | 0.8592 | 0.8717 | 0.8458 | 0.8576 |
| WD-Elman | 0.8571 | | 0.9001 | 0.8917 | 0.8768 | 0.8623 | 0.8573 |
| WD-BP | 0.8582 | | 0.8551 | 0.8872 | 0.8261 | 0.8315 | 0.8609 |
| WD-WNN | 0.8872 | | 0.9126 | 0.8276 | 0.9015 | 0.8293 | 0.8447 |
| WD-APSO-BP | 0.922 | | 0.9155 | 0.8958 | 0.9046 | 0.8952 | 0.8993 |
| WD-ACO-BP | 0.9149 | | 0.8816 | 0.8782 | 0.8979 | 0.8924 | 0.8806 |
| WD-APSOACO-BP | 0.9456 | | 0.9468 | 0.9301 | 0.9382 | 0.9299 | 0.9356 |

Note: Marked by bold is the best forecasting model

- (1) Table 6 shows the forecasting performance for each site of the three different hybrid models in 2-step forecasting in terms of six criteria: MAE, MSE, MAPE, Bias², VAR(Y), and IA. For 2-step ahead forecasting, the proposed hybrid model outperforms the other hybrid models based on each

of the evaluation criteria. For example, at Site 1, the proposed hybrid model provides a minimum forecasting error with MAE, MSE, MAPE values of 0.3490, 0.2135 and 4.79%, respectively. The IA and $Bias^2$ achieved by this hybrid model are 0.9456 and 1.1183, respectively. Compared with the 2-step ahead forecasting achieved by the other hybrid models, the forecasting performance of the proposed hybrid model is still superior.

- (2) Table 7 aims to evaluate the forecasting accuracy and stability of the proposed hybrid model in 3-step forecasting. The criterion in terms of evaluating the accuracy is the minimum MAPE values in the 1008 times experiments. This was selected to compare the accuracy of the three different hybrid models. The $Bias^2$ values of the 1008 times experiments are utilized for the stability test. In terms of the accuracy testing, the WD-APSOACO-BP obtains a lower MAPE value than the other hybrid models. The $Bias^2$ values of the proposed hybrid model always remains the lowest of the hybrid models. The proposed hybrid model obtains satisfactory forecasting stability and accuracy. In terms of the value of MAPE, the proposed hybrid model has the lowest value of MAPE among the three hybrid models. For 3-step forecasting at six sites, the proposed hybrid model obtains the smallest values of $Bias^2$ compared to the other two hybrid models.

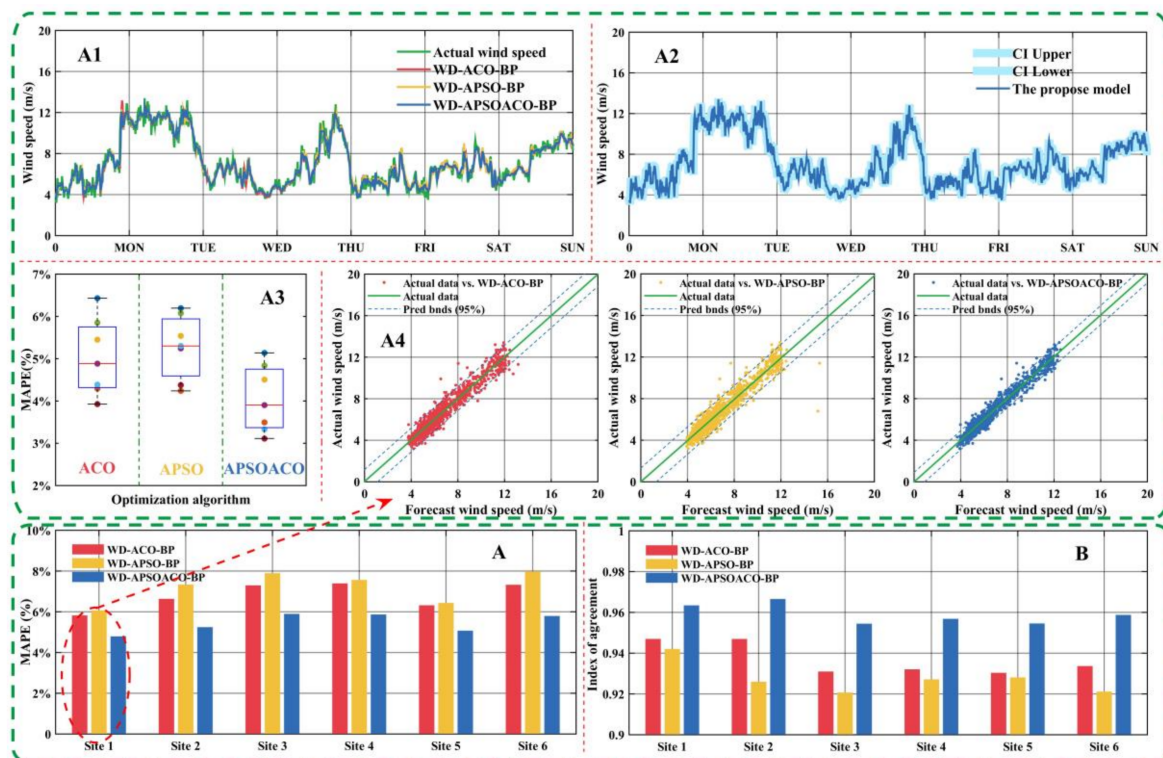


Figure 7. The forecasting results of three methods for Site 1 (2-step forecasting).

Part A3 of Figures 7 and 8 shows the MAPE and box-whisker plot of MAPE for the hybrid models of Site 3. For the 2-step and 3-step forecasting values, the proposed hybrid model obtains the lowest MAPE value. The down arrow indicates the lowest value of MAPE in the figure. Part A3 also shows that the performance of the hybrid model is better than that of the other two hybrid models. The MAPE of each point for the hybrid model is not only smaller also has a small discrete degree. Part A2 shows the 95% confidence intervals (CIs), which were obtained using the actual wind speed. The forecasting value of WD-APSOACO-BP is closer to both the upper CI and the lower CI of the observed wind speed time series. In addition, Part A.4 clearly displays the actual wind speed data compared with the forecasting results for Site 3. The multi-step (2-step and 3-step) ahead forecast values from the proposed hybrid model are closer to the target than those of multi-step (2-step and 3-step) ahead

forecasting. The minimum criteria of MAE, MSE, MAPE are generated by the hybrid model of 2-step and 3-step ahead forecasting from Site 3, respectively.

Table 7. The forecasting result of each site (3-step forecasting).

| Forecasting Model | Metric | Site | | | | | |
|-------------------|-------------------|---------------|---------------|---------------|---------------|---------------|---------------|
| | | Site 1 | Site 2 | Site 3 | Site 4 | Site 5 | Site 6 |
| WD-GRNN | MAE | 0.5527 | 0.5564 | 0.6384 | 0.6555 | 0.7058 | 0.4943 |
| WD-Elman | | 0.5550 | 0.5307 | 0.6023 | 0.6253 | 0.7103 | 0.4995 |
| WD-BP | | 0.5303 | 0.5284 | 0.6166 | 0.6405 | 0.6836 | 0.5279 |
| WD-WNN | | 0.5512 | 0.5482 | 0.5955 | 0.6523 | 0.6571 | 0.4994 |
| WD-APSO-BP | | 0.5161 | 0.5222 | 0.5825 | 0.6097 | 0.6481 | 0.487 |
| WD-ACO-BP | | 0.5246 | 0.5556 | 0.4497 | 0.6431 | 0.5677 | 0.5368 |
| WD-APSOACO-BP | | 0.4071 | 0.4303 | 0.3898 | 0.4897 | 0.4514 | 0.3834 |
| WD-GRNN | MSE | 0.5101 | 0.5044 | 0.6909 | 0.6943 | 0.8677 | 0.4683 |
| WD-Elman | | 0.5122 | 0.4811 | 0.6519 | 0.6623 | 0.8731 | 0.4733 |
| WD-BP | | 0.4894 | 0.4790 | 0.6673 | 0.6785 | 0.8403 | 0.5002 |
| WD-WNN | | 0.5087 | 0.4970 | 0.6445 | 0.6909 | 0.8077 | 0.4731 |
| WD-APSO-BP | | 0.4763 | 0.4734 | 0.6304 | 0.6458 | 0.7967 | 0.4614 |
| WD-ACO-BP | | 0.4839 | 0.5309 | 0.3535 | 0.7079 | 0.5793 | 0.5746 |
| WD-APSOACO-BP | | 0.2972 | 0.3322 | 0.293 | 0.4373 | 0.3637 | 0.2874 |
| WD-GRNN | MAPE | 8.39% | 7.33% | 9.56% | 9.34% | 9.38% | 8.34% |
| WD-Elman | | 8.42% | 6.99% | 9.02% | 8.91% | 9.44% | 8.43% |
| WD-BP | | 8.05% | 6.96% | 9.23% | 9.13% | 9.08% | 8.91% |
| WD-WNN | | 8.36% | 7.22% | 8.92% | 9.30% | 8.73% | 8.43% |
| WD-APSO-BP | | 7.83% | 6.88% | 8.72% | 8.69% | 8.61% | 8.22% |
| WD-ACO-BP | | 7.97% | 7.31% | 6.67% | 9.23% | 7.53% | 9.02% |
| WD-APSOACO-BP | | 6.15% | 5.71% | 5.86% | 6.99% | 6.03% | 6.43% |
| WD-GRNN | VAR(Y) | 0.8324 | 1.0422 | 0.8965 | 1.0480 | 0.9661 | 0.8162 |
| WD-Elman | | 0.8360 | 0.9940 | 0.8458 | 0.9997 | 0.9722 | 0.8249 |
| WD-BP | | 0.7988 | 0.9897 | 0.8659 | 1.0241 | 0.9356 | 0.8718 |
| WD-WNN | | 0.8301 | 1.0268 | 0.8363 | 1.0429 | 0.8994 | 0.8246 |
| WD-APSO-BP | | 0.7773 | 0.9781 | 0.818 | 0.9748 | 0.8871 | 0.8042 |
| WD-ACO-BP | | 0.7717 | 0.9787 | 0.8148 | 1.0174 | 0.9378 | 0.84 |
| WD-APSOACO-BP | | 0.7328 | 0.942 | 0.803 | 0.9226 | 0.7839 | 0.7756 |
| WD-GRNN | Bias ² | 1.3907 | 1.1006 | 1.4068 | 0.9545 | 1.1869 | 1.4039 |
| WD-Elman | | 1.3966 | 1.0497 | 1.3273 | 0.9104 | 1.1943 | 1.4188 |
| WD-BP | | 1.3344 | 1.0452 | 1.3587 | 0.9327 | 1.1494 | 1.4995 |
| WD-WNN | | 1.3869 | 1.0844 | 1.3123 | 0.9499 | 1.1049 | 1.4184 |
| WD-APSO-BP | | 1.2986 | 1.0329 | 1.2836 | 0.8878 | 1.0898 | 1.3832 |
| WD-ACO-BP | | 1.3632 | 1.0703 | 1.0656 | 0.9325 | 1.1069 | 1.5875 |
| WD-APSOACO-BP | | 1.2857 | 1.0043 | 1.0558 | 0.8645 | 1.0612 | 1.2428 |
| WD-GRNN | IA | 0.8227 | 0.8324 | 0.7818 | 0.7424 | 0.7524 | 0.8607 |
| WD-Elman | | 0.8193 | 0.8727 | 0.8286 | 0.7783 | 0.7477 | 0.8517 |
| WD-BP | | 0.8574 | 0.8765 | 0.8094 | 0.7598 | 0.7769 | 0.8059 |
| WD-WNN | | 0.8250 | 0.8448 | 0.8380 | 0.7460 | 0.8082 | 0.8519 |
| WD-APSO-BP | | 0.8811 | 0.8869 | 0.8568 | 0.7982 | 0.8194 | 0.8736 |
| WD-ACO-BP | | 0.8734 | 0.8729 | 0.8973 | 0.8533 | 0.8514 | 0.8431 |
| WD-APSOACO-BP | | 0.9268 | 0.9227 | 0.8993 | 0.907 | 0.9055 | 0.9207 |

Note: Marked by bold is the best forecasting model

Remark 3. From the above analysis, the best performance among the three-different hybrid forecasting models for each site is obtained by the proposed hybrid model. The proposed hybrid model provided a satisfactory forecasting performance between the WD-APSO-BP and WD-ACO-BP for 10 min wind speed multi-step forecasting. The numerical experimentation results showed that more features of the actual wind speed fluctuations can be

obtained by the proposed hybrid model, which shows a satisfactory wind speed forecasting performance at six wind farm sites.

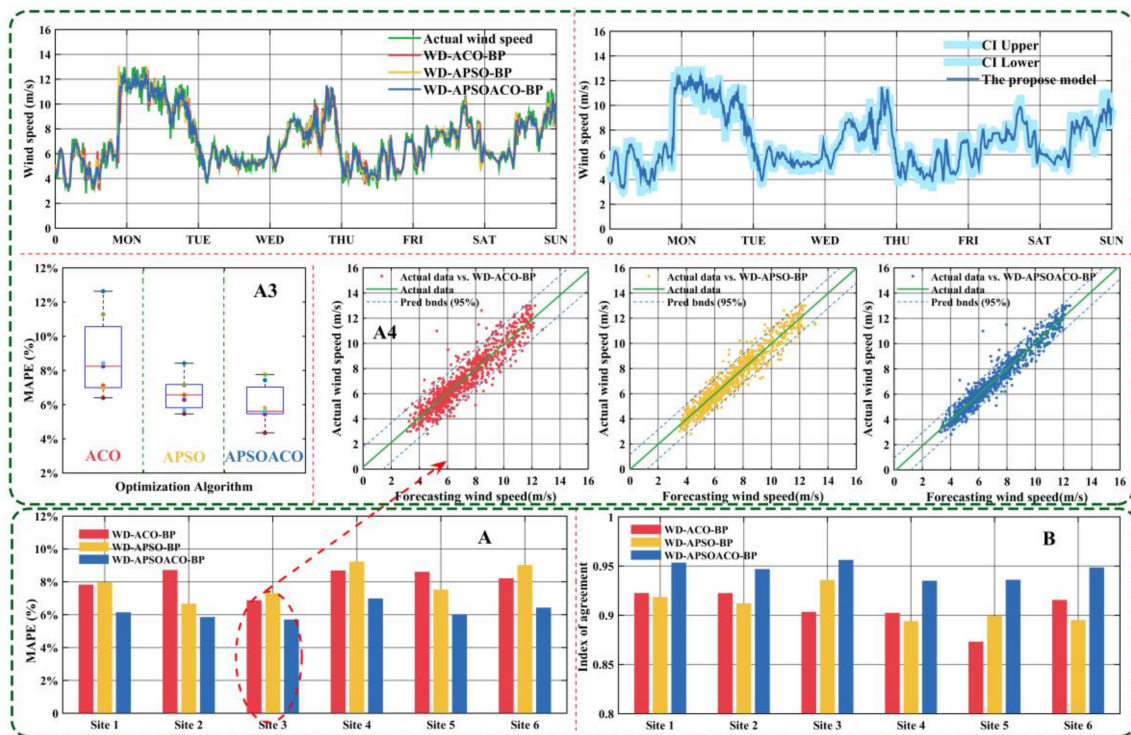


Figure 8. The forecasting results of three methods for Site 3 (3-step forecasting).

5. Discussion

In this section, the forecasting accuracy (as a reflection of the forecasting performance), the forecasting results stability of the three different hybrid models are discussed. Furthermore, the performance of each optimization algorithm is presented and discussed.

5.1. Discussion the Forecasting Accuracy of the Model

At present, the establishment of the hybrid model is mostly based on the minimum mean absolute error, mean square error, mean absolute percentage error. Such criteria and assumptions cannot be well reflected in the validity of the forecasting method. Thus, the feasibility and validity of the hybrid model are verified by two-order forecasting validity. Forecasting validity is defined as follows:

The actual value is set as $\{x_t, t = 1, 2, \dots, N\}$. m kinds of models are now used to forecast; x_{it} is the forecast value in the i th forecasting method at the j th time point ($i = 1, 2, \dots, m, t = 1, 2, \dots, N$); e_{it} is the error in the i th forecasting method at the j th time points; and $A_{it} = 1 - |e_{it}|$ is the forecasting accuracy of the i th forecasting method at the j th time point. The formula for two-order forecasting validity is $M = E(A)(1 - \sigma(A))$, where $E(A)$ represents the mathematical expectation of the forecasting accuracy of the hybrid forecasting method, $\sigma(A)$ represents the standard deviation of the prediction accuracy of the hybrid forecasting method. M is the forecasting validity. If the value of the forecasting validity is close to 1, that forecasting model is better. Table 8 indicates that the forecasting availabilities offered by the proposed hybrid model outperform those of the other models for all six sites in multi-step ahead wind speed forecasting.

Table 8. Forecasting validity of each forecasting model.

| Forecasting STEP | Forecasting Model | Site | | | | | |
|--------------------|-------------------|---------------|---------------|---------------|---------------|---------------|--------|
| | | Site 1 | Site 2 | Site 3 | Site 4 | Site 5 | Site 6 |
| 1-step forecasting | ARIMA | 0.8022 | 0.8037 | 0.8057 | 0.8099 | 0.7317 | 0.8054 |
| | ARMA | 0.7959 | 0.8314 | 0.8007 | 0.8025 | 0.7807 | 0.8046 |
| | ES(2) | 0.831 | 0.8994 | 0.8392 | 0.8337 | 0.7934 | 0.8287 |
| | ES | 0.7887 | 0.7888 | 0.7941 | 0.794 | 0.7253 | 0.7839 |
| | GRNN | 0.8115 | 0.80824 | 0.8156 | 0.8174 | 0.8092 | 0.8062 |
| | WNN | 0.9232 | 0.91915 | 0.9311 | 0.9319 | 0.9161 | 0.9271 |
| | BPNN | 0.9209 | 0.91369 | 0.9226 | 0.9257 | 0.9168 | 0.923 |
| | ElmanNN | 0.9261 | 0.91978 | 0.9284 | 0.9265 | 0.9223 | 0.9202 |
| | WD-APSO-BP | 0.9604 | 0.9702 | 0.9645 | 0.9681 | 0.9969 | 0.9932 |
| | WD-ACO-BP | 0.9572 | 0.9645 | 0.9587 | 0.9619 | 0.994 | 0.9871 |
| WD-APSOACO-BP | 0.9631 | 0.9681 | 0.9668 | 0.9711 | 0.9916 | 0.9886 | |
| 2-step forecasting | ARIMA | 0.8056 | 0.8181 | 0.8114 | 0.7424 | 0.8026 | 0.795 |
| | ARMA | 0.8058 | 0.8077 | 0.8292 | 0.8127 | 0.802 | 0.7903 |
| | ES(2) | 0.8059 | 0.8343 | 0.8389 | 0.8009 | 0.8031 | 0.7987 |
| | ES | 0.7279 | 0.7345 | 0.7988 | 0.7279 | 0.7248 | 0.7251 |
| | GRNN | 0.8088 | 0.8267 | 0.8108 | 0.8111 | 0.8062 | 0.8059 |
| | WNN | 0.9239 | 0.995 | 0.9298 | 0.9325 | 0.9265 | 0.9229 |
| | BPNN | 0.9227 | 0.9583 | 0.9318 | 0.9229 | 0.9159 | 0.9219 |
| | ElmanNN | 0.9279 | 0.9619 | 0.9317 | 0.9322 | 0.9213 | 0.9251 |
| | WD-APSO-BP | 0.9607 | 0.9667 | 0.9703 | 0.9675 | 0.9657 | 0.989 |
| | WD-ACO-BP | 0.9592 | 0.963 | 0.9596 | 0.9642 | 0.9633 | 0.9784 |
| WD-APSOACO-BP | 0.9629 | 0.9687 | 0.9654 | 0.9758 | 0.9888 | 0.9868 | |
| 3-step forecasting | ARIMA | 0.7356 | 0.8041 | 0.8108 | 0.8126 | 0.7947 | 0.73 |
| | ARMA | 0.7819 | 0.7238 | 0.8058 | 0.806 | 0.7902 | 0.7776 |
| | ES(2) | 0.7936 | 0.8349 | 0.8139 | 0.8096 | 0.8287 | 0.789 |
| | ES | 0.7278 | 0.7938 | 0.7313 | 0.733 | 0.7811 | 0.7246 |
| | GRNN | 0.8087 | 0.81331 | 0.8166 | 0.816 | 0.8015 | 0.8038 |
| | WNN | 0.9271 | 0.96123 | 0.9292 | 0.9315 | 0.9161 | 0.9199 |
| | BPNN | 0.9246 | 0.93695 | 0.9282 | 0.9315 | 0.9152 | 0.9144 |
| | ElmanNN | 0.9221 | 0.99082 | 0.925 | 0.9246 | 0.9261 | 0.9215 |
| | WD-APSO-BP | 0.9624 | 0.9639 | 0.9631 | 0.9631 | 0.9927 | 0.9823 |
| | WD-ACO-BP | 0.9515 | 0.9601 | 0.9589 | 0.9593 | 0.9874 | 0.9657 |
| WD-APSOACO-BP | 0.9645 | 0.9718 | 0.9663 | 0.9687 | 0.9805 | 0.9756 | |

Note: Marked by bold is the best forecasting model

Remark 4. The two-order validity of the forecasting model, which possesses the characteristics of high computational efficiency and less forecasting error, not only utilizes an approximate solution but also integrates a variety of forecasting methods and thus provides a more reliable index of forecasting validity.

5.2. Verification Stability of Forecasting Results

The population stability index (PSI) is the most commonly used model stability evaluation index. The formula of the population stability index is as follows:

$$PSI = \sum (Actual\% - Expected\%) \times \ln\left(\frac{Actual\%}{Expected\%}\right)$$

The expected proportion (Expected%) and the actual proportion (Actual%) represent the forecasting sample and the actual sample of the model, respectively. Generally speaking, the population stability index is less than 0.1, which represents high stability of the model. If the population stability index is greater than 0.1 and less than 0.25 the model stability is moderate, and if the population stability index is greater than 0.25 the model stability is poor. The definition of the PSI guidelines is shown in Table 9.

Table 9. The definition of population stability index (PSI) Value guidelines.

| PSI Value | Inference | Stability |
|-------------------|----------------------|------------------------------------|
| Less than 0.1 | Insignificant change | The model has high stability |
| 0.1–0.25 | Some minor change | The model stability is moderate |
| Greater than 0.25 | Major change | The stability of the model is poor |

In Table 10 and Figure 9, by comparing the WD-APSOACO-BP with two other hybrid models, we conclude that the proposed hybrid model has the most stable forecasting results. In addition, as the number of forecasting steps increases, the PSI becomes larger.

Table 10. The stability of forecasting by each model in different forecasting horizons.

| Sites | Stability (PSI) of 1-Step Forecasting | | | Stability (PSI) of 2-Step Forecasting | | | Stability (PSI) of 3-Step Forecasting | | |
|--------|---------------------------------------|--------|---------|---------------------------------------|--------|---------|---------------------------------------|--------|---------|
| | ACO | APSO | APSOACO | ACO | APSO | APSOACO | ACO | APSO | APSOACO |
| Site 1 | 0.0190 | 0.0284 | 0.0125 | 0.0210 | 0.0397 | 0.0224 | 0.0373 | 0.0708 | 0.0256 |
| Site 2 | 0.0207 | 0.0379 | 0.0192 | 0.0477 | 0.0306 | 0.0206 | 0.0551 | 0.0306 | 0.0218 |
| Site 3 | 0.0287 | 0.0185 | 0.0166 | 0.0611 | 0.0488 | 0.0191 | 0.0307 | 0.0550 | 0.0252 |
| Site 4 | 0.0059 | 0.0086 | 0.0019 | 0.0137 | 0.0253 | 0.0112 | 0.0253 | 0.0272 | 0.0192 |
| Site 5 | 0.0536 | 0.0507 | 0.0629 | 0.0907 | 0.0795 | 0.0568 | 0.0973 | 0.0937 | 0.0511 |
| Site 6 | 0.0283 | 0.0316 | 0.0232 | 0.0333 | 0.0314 | 0.0223 | 0.0495 | 0.0449 | 0.0208 |

The PSI of each model for different forecasting step

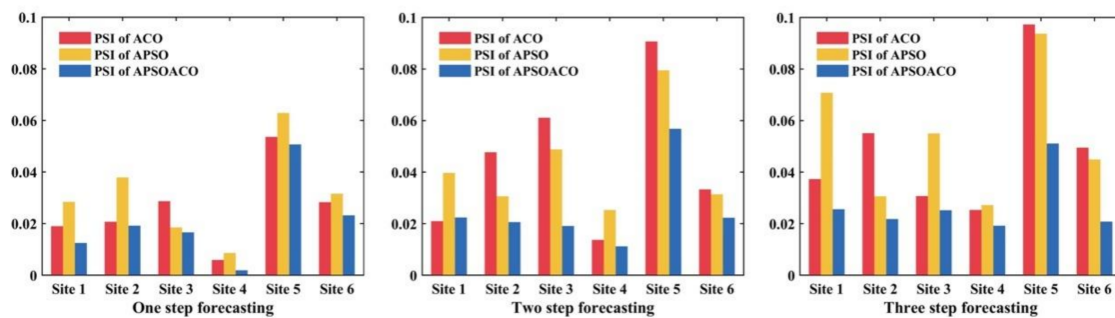


Figure 9. PSI values of different models.

Table 11 and Figure 10 show the individual calculations of the PSI for each bin. The percentage of the observations which lie in each bin are shown for both the forecasting value and the actual datasets. The PSI column shows the calculated PSI for each bin, using the formula from above. Using the guidelines as defined in Table 9, the value of the proposed hybrid forecasting model is much less than 0.1, indicating a minimal shift in the population between the actual data and the forecasting values.

Table 11. The PSI of forecasting by each model in different forecasting step in Site 1.

| Stability of One Step Forecasting | | | | | | | |
|-------------------------------------|------------|---------------------|------------|----------------------|-------------|-------------------------|----------------|
| BinEdges | Actual (%) | Expected of ACO (%) | PSI of ACO | Expected of APSO (%) | PSI of APSO | Expected of APSOACO (%) | PSI of APSOACO |
| [3, 4.1] | 3.17% | 2.08% | 0.004597 | 1.49% | 0.012778 | 2.58% | 0.001236 |
| [4.1, 5.2] | 20.44% | 21.63% | 0.000674 | 23.02% | 0.003066 | 22.02% | 0.001187 |
| [5.2, 6.3] | 23.02% | 22.72% | 3.87E-05 | 21.92% | 0.00053 | 21.73% | 0.000744 |
| [6.3, 7.4] | 16.96% | 18.95% | 0.002195 | 18.95% | 0.002195 | 18.85% | 0.001986 |
| [7.4, 8.5] | 9.13% | 7.14% | 0.004864 | 8.33% | 0.000722 | 8.04% | 0.00139 |
| [8.5, 9.6] | 9.03% | 9.33% | 9.65E-05 | 7.44% | 0.003069 | 8.13% | 0.00093 |
| [9.6, 10.7] | 6.35% | 5.95% | 0.000256 | 6.25% | 1.56E-05 | 5.95% | 0.000256 |
| [10.7, 11.8] | 7.34% | 8.43% | 0.001512 | 9.23% | 0.004308 | 9.13% | 0.003888 |
| [11.8, 12.9] | 4.17% | 3.67% | 0.000629 | 3.37% | 0.001677 | 3.57% | 0.000918 |
| [12.9, 14] | 0.40% | 0.10% | 0.004126 | 0.00% | 0.00% | 0.00% | 0 |
| | | PSI = | 0.018987 | PSI = | 0.028361 | PSI = | 0.012534 |
| Stability of two step forecasting | | | | | | | |
| BinEdges | Actual (%) | Expected of ACO (%) | PSI of ACO | Expected of APSO (%) | PSI of APSO | Expected of APSOACO (%) | PSI of APSOACO |
| [3, 4.1] | 3.17% | 2.68% | 0.000843 | 1.19% | 0.019398 | 2.28% | 0.002949 |
| [4.1, 5.2] | 20.44% | 20.24% | 1.94E-05 | 19.48% | 0.000455 | 22.12% | 0.001337 |
| [5.2, 6.3] | 23.02% | 23.51% | 0.000106 | 24.95% | 0.001561 | 22.12% | 0.000353 |
| [6.3, 7.4] | 16.96% | 19.25% | 0.002879 | 19.18% | 0.002732 | 19.05% | 0.002413 |
| [7.4, 8.5] | 9.13% | 8.53% | 0.000401 | 9.34% | 5.1E-05 | 8.53% | 0.000401 |
| [8.5, 9.6] | 9.03% | 7.74% | 0.001988 | 7.16% | 0.004344 | 7.74% | 0.001988 |
| [9.6, 10.7] | 6.35% | 5.75% | 0.000586 | 5.77% | 0.000563 | 5.36% | 0.001686 |
| [10.7, 11.8] | 7.34% | 9.13% | 0.003888 | 9.84% | 0.007325 | 9.82% | 0.007219 |
| [11.8, 12.9] | 4.17% | 3.08% | 0.003314 | 3.08% | 0.003274 | 2.98% | 0.004006 |
| [12.9, 14] | 0.40% | 0.10% | 0 | 0.00% | 0 | 0.00% | 0 |
| | | PSI = | 0.014025 | PSI = | 0.039704 | PSI = | 0.022352 |
| Stability of three step forecasting | | | | | | | |
| BinEdges | Actual (%) | Expected of ACO (%) | PSI of ACO | Expected of APSO (%) | PSI of APSO | Expected of APSOACO (%) | PSI of APSOACO |
| [3, 4.1] | 3.17% | 1.79% | 0.007991 | 0.50% | 0.049722 | 2.48% | 0.001714 |
| [4.1, 5.2] | 20.44% | 22.12% | 0.001337 | 20.93% | 0.000119 | 20.54% | 4.8E-06 |
| [5.2, 6.3] | 23.02% | 21.53% | 0.000995 | 24.40% | 0.000814 | 22.92% | 4.29E-06 |
| [6.3, 7.4] | 16.96% | 20.24% | 0.005777 | 19.74% | 0.004212 | 19.44% | 0.003384 |
| [7.4, 8.5] | 9.13% | 10.71% | 0.002545 | 7.84% | 0.001965 | 8.83% | 9.87E-05 |
| [8.5, 9.6] | 9.03% | 5.75% | 0.014746 | 7.34% | 0.003488 | 7.94% | 0.001406 |
| [9.6, 10.7] | 6.35% | 5.26% | 0.002058 | 6.94% | 0.000533 | 5.56% | 0.00106 |
| [10.7, 11.8] | 7.34% | 8.53% | 0.001789 | 9.42% | 0.005204 | 9.62% | 0.006175 |
| [11.8, 12.9] | 4.17% | 4.07% | 2.39E-05 | 2.88% | 0.004777 | 2.58% | 0.007612 |
| [12.9, 14] | 0.40% | 0.00% | 0 | 0.00% | 0 | 0.10% | 0.004126 |
| | | PSI = | 0.037262 | PSI = | 0.070834 | PSI = | 0.025586 |

Remark 5. From comparisons among the three hybrid forecasting models, it can be seen that the PSI value of the proposed hybrid model is lower than that of the others. It can be concluded that the proposed hybrid model can achieve the most stable forecasting results. In addition, as the number of forecasting steps increases, the stability of the forecasting results decreases.

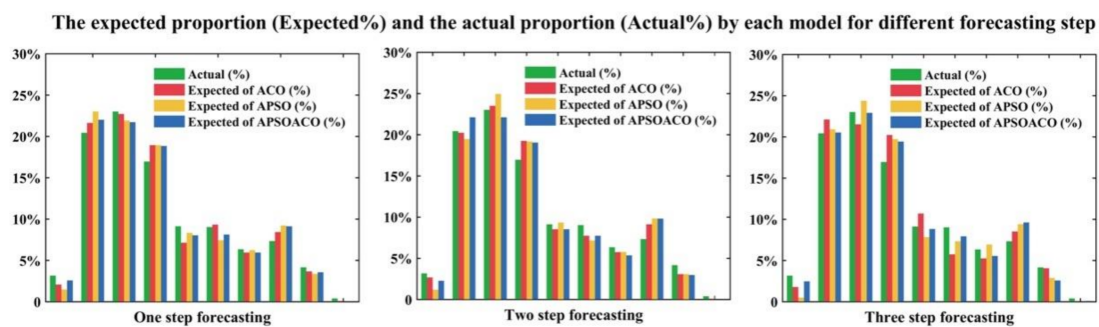


Figure 10. The expect (%) and actual (%) by each hybrid model.

5.3. Analysis of the Optimization Performance of Hybrid Optimization Algorithm

A large number of simulation experiments were undertaken for the selection of the parameters of α , β , ρ in the proposed hybrid optimization algorithm. The parameters of the ant colony optimization algorithm optimized by the adaptive particle swarm optimization algorithm are significantly different in terms of forecasting accuracy (as shown in Figure 11). The performance of the hybrid wind speed forecasting model is positively affected by the parameters in the hybrid APSOACO algorithm, which are as follows:

- (1) The inspired factor has large influence on the optimization performance and convergence of the algorithm in the hybrid APSOACO optimization. When the inspired factor is $\alpha \in [1.0, 4.0]$, the performance of the algorithm is better.
- (2) The expectation inspired factor of the APSOACO algorithm has notable influence on the performance of the algorithm and the convergence speed of the algorithm. When the expectation inspired factor is $\beta \in [3.0, 5.0]$, the performance of the algorithm is better.
- (3) The pheromone volatilization factor of the APSOACO algorithm affects the convergence of the algorithm. $1 - \rho$ is a residual factor, and when $\rho \approx 1-0.5$ (i.e., $p \approx 0.5$), the stability and performance of the algorithm is maximized. For example, in Table 12, the application of the adaptive particle swarm optimization algorithm is employed to obtain the three parameters $\alpha = 1.031792$, $\beta = 4.483219$, $\rho = 0.491852$, and these values are fed back to the parameters of the ant colony optimization algorithm. Then, the neural network is optimized for Site 1.

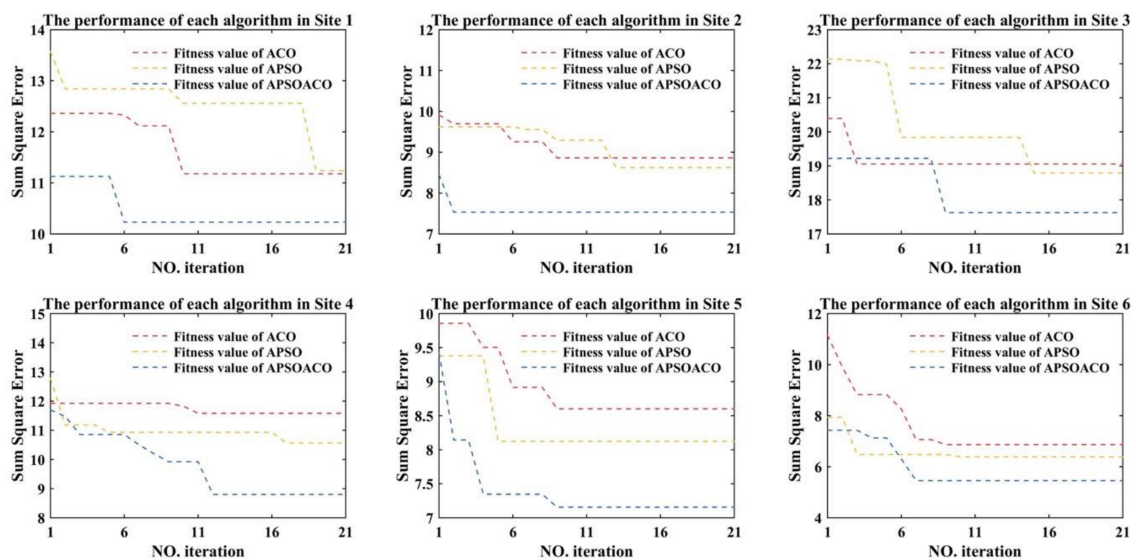


Figure 11. The performance of three different optimization algorithms.

Table 12. The optimal parameter of hybrid optimization algorithm and the optimal solution for each Site.

| Sites | Inspired Factor: α | Expectation Inspired Factor: β | Pheromone Volatilization Factor: ρ | Optimal Solution | Operation Time |
|--------|---------------------------|--------------------------------------|---|------------------|----------------|
| Site 1 | 1.031792 | 4.483219 | 0.491852 | 10.23075 | 79.92981 |
| Site 2 | 1.094882 | 4.732991 | 0.502478 | 7.876175 | 70.2076 |
| Site 3 | 1.103479 | 4.325773 | 0.47952 | 16.56985 | 70.57872 |
| Site 4 | 3.49668 | 4.759632 | 0.485673 | 9.26648 | 71.67526 |
| Site 5 | 1.009887 | 4.298647 | 0.496773 | 7.5706 | 72.82799 |
| Site 6 | 3.206893 | 4.978935 | 0.47955 | 7.513742 | 74.70964 |

Remark 6. *Through a large number of simulation experiments, the parameters of the different forecasting models are solved by the hybrid optimization algorithm. This shows that the new optimization algorithm has a higher optimization performance. It is also shown that the hybrid optimization has the ability to adaptively adjust the parameters and obtain the approximate optimal solution of the forecasting problem.*

6. Conclusions

Accurate wind speed forecasting not only plays an important role in the efficient and safe integration of wind energy into the power system, but also has benefits for the environment, economics, and social development. However, frequent fluctuations, autocorrelation, and stochastic volatility in wind speed make it difficult to obtain a satisfactory forecasting performance. In this study, a hybrid WD-APSOACO-BP model for multi-step ahead short-term wind speed forecasting is presented to overcome these problems. A data pre-processing module is exploited to eliminate the stochastic volatility and fully extract the main features of wind speed by removing small fluctuations and retaining only useful information, as well as creating conditions for improvement of the forecasting accuracy. A hybrid APSOACO algorithm which avoids the limitations caused by subjective setting parameters is utilized to tune and optimize the parameters of the BP neural network in the optimization module. Then, a set of high quality parameters is calculated and applied to optimize the parameters of the BP neural network in the forecasting module. In the evaluation module, experiments from six wind speed data sites in China clearly indicate that the proposed hybrid model is superior to the other alternative models that were explored in this paper. In addition to single-step ahead forecasting, multi-step ahead wind speed forecasting is also adopted and discussed in this paper. The obtained testing results with respect to different forecasting horizons suggest that the developed hybrid wind speed forecasting approach based on the BP neural network integrated with the APSOACO algorithm has the ability to yield satisfactory wind speed forecasting accuracy.

Author Contributions: Chen Wang. conceived and designed the experiments; Chen Wang performed the experiments; Chen Wang and Zonggui Yao. analyzed the data; Chen Wang contributed reagents/materials/analysis tools; Chen Wang wrote the paper.

Acknowledgments: This research was supported by the National Natural Science Foundation of China (Grant No. 71171102/G0107).

Conflicts of Interest: The authors declare no conflict of interest.

Nomenclature

| | |
|--------|---|
| RESs | renewable energy sources |
| GWEC | global wind energy council |
| ARMA | auto regressive moving average |
| ARIMA | auto regressive integrated moving average |
| GARCH | generalized autoregressive conditional heteroscedasticity |
| ANN | artificial neural networks |
| BP | back propagation |
| GRNN | general regression neural network |
| RBFINN | radial basis function neural network |
| DBN | deep belief network |
| EEMD | ensemble empirical mode decomposition |
| GA | genetic algorithm |
| EMD | empirical mode decomposition |
| SVR | support vector machine |
| IMF | intrinsic mode function |
| WPD | wavelet packet decomposition |
| COA | crisscross optimization algorithm |
| ELM | extreme learning machine |

| | |
|----------|---|
| HBSA | hybrid backtracking search algorithm |
| WD | wavelet de-noising |
| ACO | ant colony optimization |
| ACO | ant colony optimization |
| APSO | adaptive particle swarm optimization |
| APSOACO | a modified adaptive particle swarm optimization algorithm based ant colony optimization algorithm |
| WTT | wavelet transforms technique |
| CWT | continuous wavelet transforms |
| DWT | discrete wavelet transforms |
| IFS | iterated function system |
| RM | rolling mechanism |
| AE | average error |
| MAE | mean absolute error |
| MAPE | mean absolute percentage error |
| BPNN | back propagation neural network |
| Elman NN | Elman neural network |
| WNN | wavelet neural network |
| ES | exponential smoothing |
| dbN | N-order Daubechies wavelet |
| IA | Index Agreement |
| CI | confidence interval |
| PSI | population stability index |
| ELM | extreme learning machine |
| ACO | ant colony optimization |

References

- Hu, J.; Wang, J.; Xiao, L. A hybrid approach based on the gaussian process with t-observation model for short-term wind speed forecasts. *Renew. Energy* **2017**, *114*, 670–685. [[CrossRef](#)]
- REN21 Renewables 2012 Global Status Report; REN21 Secretariat: Paris, France, 2012.
- World Wind Market has Reached 486 GW from Where 54 GW has been Installed Last Year. Available online: <http://www.wwindea.org/11961-2/> (accessed on 5 March 2018).
- Zhang, Z.S.; Sun, Y.Z.; Cheng, L. Potential of trading wind power as regulation services in the California short-term electricity market. *Energy Policy* **2013**, *9*, 885–897. [[CrossRef](#)]
- Tascikaraoglu, A.; Uzunoglu, M. A review of combined approaches for prediction of short-term wind speed and power. *Renew. Sustain. Energy Rev.* **2014**, *34*, 243–254. [[CrossRef](#)]
- Wang, J.; Heng, J.; Xiao, L.; Wang, C. Research and application of a combined model based on multi-objective optimization for multi-step ahead wind speed forecasting. *Energy* **2017**, *125*, 591–613. [[CrossRef](#)]
- Giorgi, M.G.D.; Ficarella, A.; Tarantino, M. Assessment of the benefits of numerical weather predictions in wind power forecasting based on statistical methods. *Energy* **2011**, *36*, 3968–3978. [[CrossRef](#)]
- Cassola, F.; Burlando, M. Wind speed and wind energy forecast through kalman filtering of numerical weather prediction model output. *Appl. Energy* **2012**, *99*, 154–166. [[CrossRef](#)]
- Erdem, E.; Shi, J. Arma based approaches for forecasting the tuple of wind speed and direction. *Appl. Energy* **2011**, *88*, 1405–1414. [[CrossRef](#)]
- Kavasseri, R.G.; Seetharaman, K. Day-ahead wind speed forecasting using f-arima models. *Renew. Energy* **2009**, *34*, 1388–1393. [[CrossRef](#)]
- Shen, Z.; Ritter, M. Forecasting volatility of wind power production. *Appl. Energy* **2016**, *176*, 295–308. [[CrossRef](#)]
- Chang, S.G.; Yu, B.; Vetterli, M. Spatially adaptive wavelet thresholding with context modeling for image denoising. *IEEE Trans. Image Process.* **2000**, *9*, 1522–1531. [[CrossRef](#)] [[PubMed](#)]
- Tascikaraoglu, A.; Sanandaji, B.M.; Poolla, K.; Varaiya, P. Exploiting sparsity of interconnections in spatio-temporal wind speed forecasting using wavelet transform. *Appl. Energy* **2016**, *165*, 735–747. [[CrossRef](#)]

14. Weron, R. Electricity price forecasting: A review of the state-of-the-art with a look into the future. *Int. J. Forecast.* **2014**, *30*, 1030–1081. [[CrossRef](#)]
15. Amjady, N.; Keynia, F. Day ahead price forecasting of electricity markets by a mixed data model and hybrid forecast method. *Int. J. Electr. Power Energy Syst.* **2008**, *30*, 533–546. [[CrossRef](#)]
16. Guo, Z.H.; Wu, J.; Lu, H.Y.; Wang, J.Z. A case study on a hybrid wind speed forecasting method using bp neural network. *Knowl. Based Syst.* **2011**, *24*, 1048–1056. [[CrossRef](#)]
17. Zhao, W.; Wei, Y.M.; Su, Z. One day ahead wind speed forecasting: A resampling-based approach. *Appl. Energy* **2016**, *178*, 886–901. [[CrossRef](#)]
18. Chen, B.; Zhao, L.; Wang, X.; Lu, J.H.; Liu, G.Y.; Cao, R.F.; Liu, J. Wind speed prediction using ols algorithm based on rbf neural network. In Proceedings of the IEEE Power and Energy Engineering Conference (APPEEC 2009), Wuhan, China, 27–31 March 2009.
19. Wang, H.Z.; Wang, G.B.; Li, G.Q.; Peng, J.C.; Liu, Y.T.; Yan, J. Deep belief network based deterministic and probabilistic wind speed forecasting approach. *Appl. Energy* **2016**, *182*, 80–93. [[CrossRef](#)]
20. Cadenas, E.; Rivera, W. Wind speed forecasting in three different regions of Mexico, using a hybrid ARIMA–ANN model. *Renew. Energy* **2010**, *35*, 2732–2738. [[CrossRef](#)]
21. Liu, H.; Tian, H.Q.; Pan, D.F.; Li, Y.F. Forecasting models for wind speed using wavelet, wavelet packet, time series and artificial neural networks. *Appl. Energy* **2013**, *107*, 191–208. [[CrossRef](#)]
22. Du, P.; Jin, Y.; Zhang, K. A hybrid multi-step rolling forecasting model based on ssa and simulated annealing—Adaptive particle swarm optimization for wind speed. *Sustainability* **2016**, *8*, 754. [[CrossRef](#)]
23. Ma, X.; Jin, Y.; Dong, Q. A generalized dynamic fuzzy neural network based on singular spectrum analysis optimized by brain storm optimization for short-term wind speed forecasting. *Appl. Soft Comput.* **2017**, *54*, 296–312. [[CrossRef](#)]
24. Wang, S.; Zhang, N.; Wu, L.; Wang, Y. Wind speed forecasting based on the hybrid ensemble empirical mode decomposition and GA-BP neural network method. *Renew. Energy* **2016**, *94*, 629–636. [[CrossRef](#)]
25. Ren, Y.; Suganthan, P.N.; Srikanth, N. A novel empirical mode decomposition with support vector regression for wind speed forecasting. *IEEE Trans. Neural Netw. Learn. Syst.* **2016**, *27*, 1793–1798. [[CrossRef](#)] [[PubMed](#)]
26. Zhang, C.; Zhou, J.; Li, C.; Fu, W.; Peng, T. A compound structure of ELM based on feature selection and parameter optimization using hybrid backtracking search algorithm for wind speed forecasting. *Energy Convers. Manag.* **2017**, *143*, 360–376. [[CrossRef](#)]
27. Zhang, C.; Wei, H.; Zhao, J.; Liu, T.; Zhu, T.; Zhang, K. Short-term wind speed forecasting using empirical mode decomposition and feature selection. *Renew. Energy* **2016**, *96*, 727–737. [[CrossRef](#)]
28. Moghram, I.; Rahman, S. Analysis and evaluation of five short-term load forecasting techniques. *IEEE Trans. Power Syst.* **2002**, *4*, 1484–1491. [[CrossRef](#)]
29. Goswami, J.C.; Chan, A.K. *Fundamentals of Wavelets: Theory, Algorithms and Applications*; Wiley: Hoboken, NJ, USA, 2011.
30. Wang, J.Z.; Wang, J.J.; Zhang, Z.G.; Guo, S.P. Forecasting stock indices with back propagation neural network. *Expert Syst. Appl.* **2011**, *38*, 14346–14355. [[CrossRef](#)]
31. Xiao, L.; Wang, J.; Dong, Y.; Wu, J. Combined forecasting models for wind energy forecasting: a case study in China. *Renew. Sustain. Energy Rev.* **2015**, *44*, 271–288. [[CrossRef](#)]
32. Sun, W.; Xu, Y. Financial security evaluation of the electric power industry in china based on a back propagation neural network optimized by genetic algorithm. *Energy* **2016**, *101*, 366–379. [[CrossRef](#)]
33. Section, T. Short-term wind speed hybrid forecasting model based on bias correcting study and its application. *Math. Probl. Eng.* **2015**, *2015*, 1–13.
34. Navascués, M.A.; Sebastián, M.V. Smooth fractal interpolation. *J. Inequal. Appl.* **2006**, *2006*, 78734. [[CrossRef](#)]
35. Zhan, Z.H.; Zhang, J. Adaptive particle swarm optimization. In *Ant Colony Optimization and Swarm Intelligence*; Springer: Berlin/Heidelberg, Germany, 2008; pp. 227–234.
36. Shen, Q.; Jiang, J.H.; Tao, J.C.; Shen, G.L.; Yu, R.Q. Modified ant colony optimization algorithm for variable selection in QSAR modeling: QSAR studies of cyclooxygenase inhibitors. *Cheminform* **2005**, *45*, 1024–1029.
37. Stützle, T. Ant colony optimization. *Comput. Intell. Mag. IEEE* **2003**, *1*, 28–39.
38. Jiang, P.; Liu, F.; Wang, J.; Song, Y. Cuckoo search-designated fractal interpolation functions with winner combination for estimating missing values in time series. *Appl. Math. Modell.* **2016**, *40*, 9692–9718. [[CrossRef](#)]
39. Lu, C.J. Integrating independent component analysis-based denoising scheme with neural network for stock price prediction. *Expert Syst. Appl.* **2010**, *37*, 7056–7064. [[CrossRef](#)]

40. Aussem, A.; Campbell, J.; Murtagh, F. Wavelet-based feature extraction and decomposition strategies for financial forecasting. *J. Comput. Intell. Financ.* **1998**, *6*, 5–12.
41. Zheng, G.; Starck, J.L.; Campbell, J.; Murtagh, F.; Zheng, G.; Campbell, J. The wavelet transform for filtering financial data streams. *J. Comput. Intell. Finance* **1999**, *7*, 18–35.
42. Zhang, J.; Morris, A.J. A sequential learning approach for single hidden layer neural networks. *Neural Netw.* **1998**, *11*, 65–80. [[CrossRef](#)]
43. Niu, T.; Wang, J.; Zhang, K.; Du, P. Multi-step-ahead Wind Speed Forecasting Based on Optimal Feature Selection and a Modified Bat Algorithm with the Cognition Strategy. *Renew. Energy* **2017**, *118*, 213–229. [[CrossRef](#)]
44. Liu, L.; Wang, Q.; Wang, J.; Liu, M. A rolling grey model optimized by particle swarm optimization in economic prediction. *Comput. Intell.* **2016**, *32*, 391–419. [[CrossRef](#)]
45. Jolayemi, E.T. A Multiraters Agreement Index for Ordinal Classification. *Biom. J.* **1991**, *33*, 485–492. [[CrossRef](#)]
46. Yu, L.; Lai, K.K.; Wang, S.; Huang, W. A Bias-Variance-Complexity Trade-Off Framework for Complex System Modeling. In *Computational Science and Its Applications—ICCSA 2006*; Springer: Berlin/Heidelberg, Germany, 2006.



© 2018 by the authors. Licensee MDPI, Basel, Switzerland. This article is an open access article distributed under the terms and conditions of the Creative Commons Attribution (CC BY) license (<http://creativecommons.org/licenses/by/4.0/>).